Calhoun: The NPS Institutional Archive

DSpace Repository

Theses and Dissertations | 1. Thesis and Dissertation Collection, all items

1981-06

Tropical storm movement based on synoptic map typing using empirical orthogonal functions

Brown, Danley W.

http://hdl.handle.net/10945/20699

Downloaded from NPS Archive: Calhoun

http://www.nps.edu/library

Calhoun is the Naval Postgraduate School's public access digital repository for research materials and institutional publications created by the NPS community. Calhoun is named for Professor of Mathematics Guy K. Calhoun, NPS's first appointed -- and published -- scholarly author.

Dudley Knox Library / Naval Postgraduate School
411 Dyer Road / 1 University Circle
Monterey, California USA 93943

TROPICAL STORM MOVEMENT BASED ON SYNOPTIC MAP TYPING USING EMPIRICAL ORTHOGONAL FUNCTIONS

Danley W. Brown

NAVAL POSTGRADUATE SCHOOL
Monterey, California

THESIS

TROPICAL STORM MOVEMENT BASED ON SYNOPTIC MAP TYPING USING EMPIRICAL ORTHOGONAL FUNCTIONS

by

Danley W. Brown

June 1981

Thesis Advisor: R. L. Elsberry

Approved for public release; distribution unlimited.

T199886

SECURITY CLASSIFICATION OF THIS PAGE (When Data Entered)

REPORT DOCUMENTATION PAGE

READ INSTRUCTIONS BEFORE COMPLETING FORM

1. REPORT NUMBER	2. GOVT ACCESSION NO. / 3. RECIPIENT'S CATALOG NUMBER
4. TITLE (and Subtitle): Tropical Storm Movement Based on Synoptic Map Typing Using Empirical Orthogonal Functions	5. TYPE OF REPORT & PERIOD COVERED: Master's Thesis; June 1981
	6. PERFORMING ORG. REPORT NUMBER
7. AUTHOR(s): Danley W. Brown	8. CONTRACT OR GRANT NUMBER(s)
9. PERFORMING ORGANIZATION NAME AND ADDRESS: Naval Postgraduate School, Monterey, California 93940	10. PROGRAM ELEMENT, PROJECT, TASK AREA & WORK UNIT NUMBERS
11. CONTROLLING OFFICE NAME AND ADDRESS: Naval Postgraduate School, Monterey, California 93940	12. REPORT DATE: June 1981
	13. NUMBER OF PAGES: 80
14. MONITORING AGENCY NAME & ADDRESS(if different from Controlling Office)	15. SECURITY CLASS. (of this report): Unclassified
	15a. DECLASSIFICATION/DOWNGRADING SCHEDULE

16. DISTRIBUTION STATEMENT (of this Report)

Approved for public release; distribution unlimited.

17. DISTRIBUTION STATEMENT (of the abstract entered in Block 20, if different from Report)

18. SUPPLEMENTARY NOTES

19. KEY WORDS (Continue on reverse side if necessary and identify by block number)

Map Typing
Empirical Orthogonal Function Analysis
Tropical Storm Movement

20. ABSTRACT (Continue on reverse side if necessary and identify by block number)

This initial study investigates the feasibility of using weather map types to forecast tropical storm/typhoon movement in the Western North Pacific Ocean. Fleet Numerical Oceanographic Center's hemispheric D-value analysis fields at 850, 700 and 500 mb are interpolated to a standard grid oriented relative to the present surface tropical storm position. Empirical Orthogonal Function (EOF) analysis is used to represent

DD FORM 1 JAN 73 1473 EDITION OF 1 NOV 65 IS OBSOLETE
S/N 0102-014-6601

the fields in terms of only 10 coefficients in an effort to separate true synoptic map features from random noise. A least squares approach is then applied to determine characteristic synoptic patterns relative to the tropical storm, and to relate each individual case to a "map type". An analog type approach is used to forecast the 30-, 36-, 54-, 60-, 78- and 84-hour positions. All storms determined to be of the same map type as the candidate storm were considered to be analogs, and their storm tracks were rotated to have the same past 12-hour movement. Forecast errors ranged from 135 n.mi. at 30 hours to 490 n.mi. at 84 hours. Although no independent cases were tested, and the techniques employed have not been optimized, the mean vector errors indicate that the basic technique warrants further investigation.

Approved for public release; distribution unlimited.

Tropical Storm Movement Based on Synoptic Map Typing Using Empirical Orthogonal Functions

by

Danley W. Brown
Major, United States Air Force
B.S., Grove City College, 1969
B.S., Pennsylvania State University, 1970

Submitted in partial fulfillment of the
requirements for the degree of

MASTER OF SCIENCE IN METEOROLOGY

from the

NAVAL POSTGRADUATE SCHOOL
June 1981

ABSTRACT

This initial study investigates the feasibility of using weather map types to forecast tropical storm/typhoon movement in the Western North Pacific Ocean. Fleet Numerical Oceanographic Center's hemispheric D-value analysis fields at 850, 700 and 500 mb are interpolated to a standard grid oriented relative to the present surface tropical storm position. Empirical Orthogonal Function (EOF) analysis is used to represent the fields in terms of only 10 coefficients in an effort to separate true synoptic map features from random noise. A least squares approach is then applied to determine characteristic synoptic patterns relative to the tropical storm, and to relate each individual case to a "map type". An analog type approach is used to forecast the 30-, 36-, 54-, 60-, 78- and 84-hour positions. All storms determined to be of the same map type as the candidate storm were considered to be analogs, and their storm tracks were rotated to have the same past 12-hour movement. Forecast errors ranged from 135 n.mi. at 30 hours to 490 n.mi. at 84 hours. Although no independent cases were tested, and the techniques employed have not been optimized, the mean vector errors indicate that the basis technique warrants further investigation.

TABLE OF CONTENTS

I. INTRODUCTION - 10

II. DATA ACQUISITION AND EMPIRICAL ORTHOGONAL FUNCTION ANALYSIS - - - - - - - - - - - - - - - - 14

A. STORM SELECTION - - - - - - - - - - - - - - - - 14

B. DATA NORMALIZATION - - - - - - - - - - - - - - 18

C. EMPIRICAL ORTHOGONAL FUNCTION (EOF) ANALYSIS - - - - - - - - - - - - - - - - 23

III. MAP TYPING - 32

IV. ANALOG TRACK FORECASTS BY MAP TYPES - - - - - - - 49

V. SUGGESTED IMPROVEMENTS - - - - - - - - - - - - - - 55

VI. SUMMARY - 60

APPENDIX A - 62

APPENDIX B - 66

APPENDIX C - 67

APPENDIX D - 73

LIST OF REFERENCES - - - - - - - - - - - - - - - - - - - 77

INITIAL DISTRIBUTION LIST - - - - - - - - - - - - - - - 79

LIST OF TABLES

I. Number of cases available per forecast time interval - - - - - - - - - - - - - - - - - - - 17

II. Cumulative percent of variance and the actual variance (m^2) or eigenvalue as expressed by the linear combination of eigenvectors for each level. An arbitrary cutoff at 10 eigenvectors was used here - 29

III. Summary of mean forecast errors (n.mi.) and standard deviations (n.mi.) for the analog-type forecast - - - - - - - - - - - - - - - 51

IV. Mean forecast errors (n.mi.) and standard deviations (n.mi.) by 500 mb map type and forecast interval - - - - - - - - - - - - - - - - 52

V. 20 examples of 30-hour forecasts made at 850, 700 and 500 mb. All positions are relative to the standardized 0-hour position (10° N, 140° E) and given as lat/long (map type number) - - - - - - - - - - - - - - 54

VI. 30-hour forecast mean errors (n.mi.) and standard deviations (n.mi.) at 500 mb using 20 terms of the EOF - - - - - - - - - - - - 56

C1. 850 mb errors and standard deviations (n.mi.) by map type and forecast interval - - - - - - - - 69

C2. 700 mb errors and standard deviations (n.mi.) by map type and forecast interval - - - - - - - - 72

LIST OF FIGURES

1. The standard grid used to plot the D-value fields. The standard position of the storm on every map is at position 70 - - - - - - - - - 12

2. The forecasts 1, 2, 3 and 4 represent the 4 scheduled warnings issued by JTWC each day. The X marks upper level analysis time; o represents time that forecasts would be available from this research, * represents the time warnings are issued; and $ represents warning forecast times. This diagram illustrates the reason for the 30-, 36-, 54-, 60-, 78- and 84-hour forecast intervals - - - - - 17

3. This is a very generalized picture of the flow as it appears on the grid. Note the difference in speed, relative to the storm, of features to the north of the storm compared to features south of the storm - - - - - - 18

4. The effect of the different normalization schemes at 500 mb. The four representations are for 00 GMT, 18 Mar 1967. A is the actual field; B, C and D are the EOF representations (truncated at 10 terms) using grid-point normalization, whole field normalization and map normalization, respectively. The isopleths are D-values (m) - - - - - 20

5. Similar to Fig. 4 except for 12 GMT 25 Aug 1967 - - - - - - - - - - - - - - - - - - 21

6. The D-value means (left side) and standard deviations (right side) for 850 mb (bottom), 700 mb (middle) and 500 mb (top). The isopleths are D-values (m) - - - - - - - - - - - 24

7. An example of the effect of truncation of the EOF for 00 GMT, 18 Mar 1967. The number above the map is the number of terms included (the truncation point). The isopleths are D-values (m) - - - - - - - - - - - 30

8. The 500 mb map types. The number above each map refers to the map type number, i.e. in the order selected. Isopleths are D-values (m) - - - - - - - - - - - - - - - - - - 36

9. Examples of map type 2 (500 mb). The letters above the maps are for reference for the text. The isopleths are D-values (m) - - 41

10. Examples of map type 1 (500 mb). The letters above the maps are for reference for the text. The isopleths are D-values (m) - - 42

11. The 500 mb map types using 20 terms of the EOF. The number above the maps refer to the map type number. The isopleths are D-values (m) - 45

C1. 850 mb map types 1-6. Isopleths are D-values (m) - - - - - - - - - - - - - - - - - - - 67

C2. 700 mb map types 1-6. Isopleths are D-values (m) - - - - - - - - - - - - - - - - - - - 70

D1. Examples of 500 mb maps. Isopleths are D-values (m) and the classification by map type is indicated by the number above the map type - - - - - - - - - - - - - - - - 73

ACKNOWLEDGEMENTS

I would like to express my sincere thanks to Prof. R. L. Elsberry for his patience, guidance and assistance throughout the course of this research. Also, Dr. R. L. Haney's interest and constructive comments were greatly appreciated.

I am indebted to Systems and Applied Sciences Corporation for providing the data upon which this research is based. I am grateful to Fleet Numerical Oceanographic Center (FNOC) for allowing me to use their busy computer facilities. James Peak's assistance in using the FNOC computer and in constructing the data base was greatly appreciated. I want to sincerely thank Lieutenant Scott Sandgathe (USN) for his interest in my research, particularly for providing an attentive ear for my many attempts to explain Empirical Orthogonal Functions as I struggled to use them and understand how they worked.

Finally, I am extremely grateful to my wife, Duen, for her patience and understanding during the long hours spent on this research, and to my children for letting Daddy do his "homework", without too many interruptions.

I. INTRODUCTION

Neumann (1979) states that the temporal and spatial analysis of tropical cyclone paths show a tendency to be repetitive, and to be associated with identifiable weather patterns. Experienced tropical cyclone forecasters routinely examine the synoptic fields for the position of the subtropical ridge, any weakness in the intensity of the ridge, locations of migratory troughs in the mid-latitudes and any other synoptic features that may give indications of future storm movement. In a series of lectures at the Naval Postgraduate School, Dr. William M. Gray, Colorado State University, indicated that much more can be done to examine how tropical storms react to their environment. In addition, he stated that more immediate gains in forecasting storm movement would come from examining the surrounding synoptic fields than from detailed modeling of the inner core of the storm. He bases this assessment on the fact that for at least the foreseeable future, detailed data in the immediate vicinity of the storm will not be available. Furthermore, with continued advances in satellite sensors and satellite interpretation, data will be available to better define the environment around the storm, if not the inner circulation.

This research is an initial study to determine the feasibility of applying a synoptic map-typing scheme to the problem of forecasting tropical storms in the Western North Pacific Ocean. The basic concept is that tropical storm movement is directly related to the forcing of the general synoptic height field in which it is embedded, and that this forcing can be represented by a set of map types. Because of time limitations, the techniques applied could not be optimized. Rather, the aim is to demonstrate that the basic concept is sound, before perfecting the technique and adding the detailed refinements typical of other analog schemes.

Analog techniques typically involve relating the current storm with historical storms that are temporally and spatially similar. Among the parameters used in the Atlantic Ocean by Hope and Neumann (1970) and in the Pacific Ocean by Jarrell and Somervell (1970) are distances to the subtropical ridge and to the nearest trough. Instead of deriving such subjective parameters, this study directly uses the synoptic fields to objectively determine which relationships are the important ones. Tse (1966) attempted a similar study, in which he subjectively developed five groups of map types. He successfully used these to stratify his sample cases prior to developing a pressure gradient nomogram to predict typhoon movement.

In this study, analyzed D-value (deviations from standard heights at specific pressure levels) fields were obtained from Systems and Applied Sciences Corporation, Monterey, CA. A total of 504 individual cases, from 1 January 1967 to 31 December 1976, were interpolated to a standard grid (see Fig. 1). Since map types must be constructed from synoptic situations relative to the tropical storm, this grid had to be movable in space so that the storm is always located in the same position. In each case the 850, 700 and 500 mb fields were utilized to determine which specific level provided the best steering information.

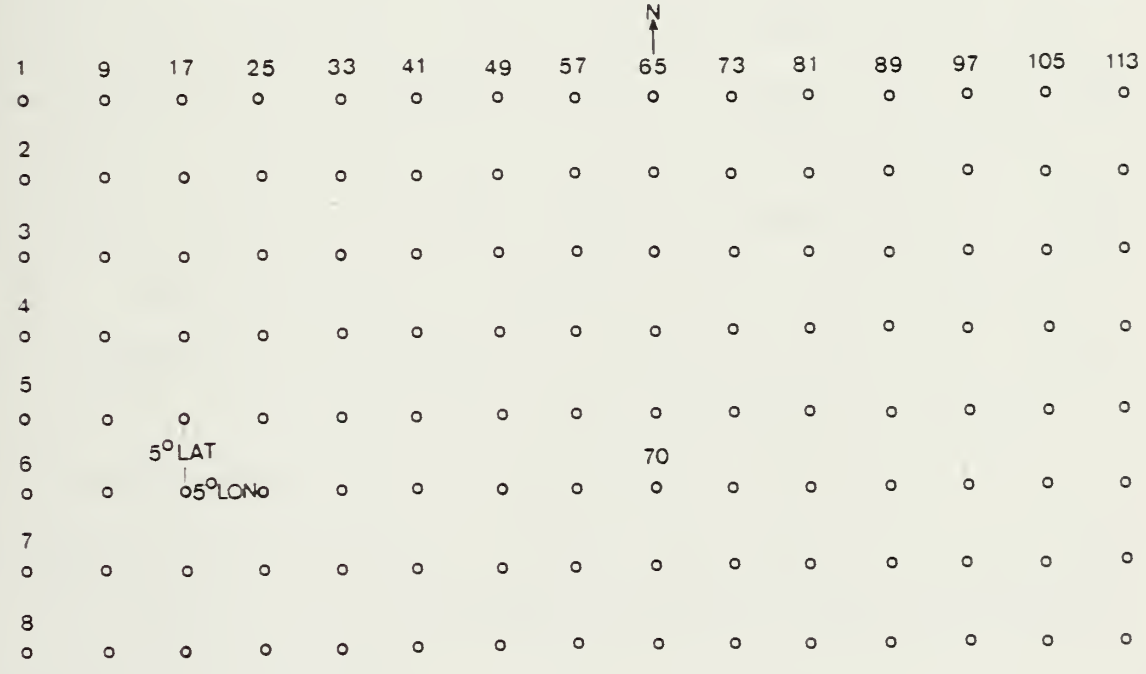

Figure 1: The standard grid used to plot the D-value fields. The standard position of the storm on every map is at position 70.

Empirical Orthogonal Function (EOF) analysis was used for two reasons. First, it can be used to separate the random noise from the true synoptic patterns. Secondly, it can be used to reduce the number of descriptors required to describe the synoptic field from the 120 grid points to a smaller number of EOF coefficients. Map types were selected using least squares statistics from the EOF representations of the D-value fields surrounding the 504 storm cases. The basic procedure is analogous to that of Lund (1963). Each of the historical fields is then screened a second time to assign it to one of the selected map types.

As a preliminary test of the usefulness of this map typing, a forecast position is derived using archived best-track storm positions. Each forecast storm position is derived from an unweighted average of best-track positions (rotated so that each case has the same movement for the previous 12 hours) for all the other storms within the map type. This procedure is applied to all three levels and six forecast time intervals. The results are then used to support the hypothesis that storm movement is related to the surrounding synoptic height field. Finally, several suggestions are made for further improvements to this technique, and for using the basic concept to develop another type of analog scheme.

II. DATA ACQUISITION AND EMPIRICAL ORTHOGONAL FUNCTION ANALYSIS

A. STORM SELECTION

Data from a ten-year period from 1 January 1967 to 31 December 1976 form the sample. All storms between 1 October 1972 and 31 December 1972, and 7 September 1973 to 31 December 1973 had to be omitted because the D-value fields were not available. Only two historical data sets, the best-track storm data and the upper-level D-value analysis fields, were required. Both sets were available from the Fleet Numerical Oceanographic Center's (FNOC) archive files.

The actual selection of the 504 case studies was made on the basis of the following criteria:

(1) The storm had to be at least tropical storm strength, with a maximum wind speed in excess of 35 knots;

(2) The storm had to have at least 12 hours of prior track and persist for at least 30 hours;

(3) Only 00 GMT and 12 GMT initial storm positions were considered since upper-level analysis fields are only available at these times;

(4) Each case had to have all three levels (850, 700 and 500 mb) of data;

(5) To insure independent samples of gridded D-value maps relative to the same storm, each case had to be at least 36 hours apart. However, this restriction did not exclude data from a second storm occurring on the same date, because each case would be gridded according to its own location, and would therefore represent independent samples; and

(6) All storms located south of 10° N lat were eliminated since that would extend the grid into the Southern Hemisphere.

A standard grid was required that could be relocated based on the position of the tropical storm. Neumann (1979) presents a grid that has been frequently used in Atlantic tropical cyclone forecast models. We selected a similar 8 x 15 grid and positioned the storm center at the 70 position (see Fig. 1), since most storms have a west-northwest movement. The storm center and grid were located in the FNOC 63 x 63 hemispheric analysis fields and the D-values were interpolated to the grid points using the BSSLG subroutine from the FNOC computer library. This subroutine interpolates a data field of dimensions (M x N) for a point using Bessel's central difference formula.

Best-track storm positions are collected every 6 hours, beginning 12 hours prior to the forecast time and extending to + 84 hours. Since upper-level data fields are only

available at 00 GMT and 12 GMT, map typing can be done only twice each day. Because the analysis fields are not available until about 03 GMT and 15 GMT, a 24-hour forecast from map time would only be an 18-hour forecast by the time the Joint Typhoon Warning Center (JTWC) could use it to prepare a warning. On the basis of these considerations, forecasts are made at 30, 36, 54, 60, 78 and 84 hours from analysis time, with new forecasts available for the 06 GMT and 18 GMT warnings (see Fig. 2). In Table I, the 504 cases are broken down by the number of cases in the sample with sufficient best-track data to be useful in developing the analog forecast positions.

An alternate approach of using the most recent upper-level analysis with the current storm position (+6 or +12 hours from analysis time) was considered unsatisfactory for two reasons. First, there would always be a discrepancy between the present storm position and the actual position of the low pressure center in the map. Elimination of this discrepancy would require smoothing in the region of the prior storm position and the introduction of a bogus storm at the present position. Secondly and most importantly, the synoptic conditions to the north of the storm that may affect storm motion are generally moving in the opposite direction of the tropical storm (see Fig. 3). Therefore, the synoptic pattern north of the storm would generally be translating

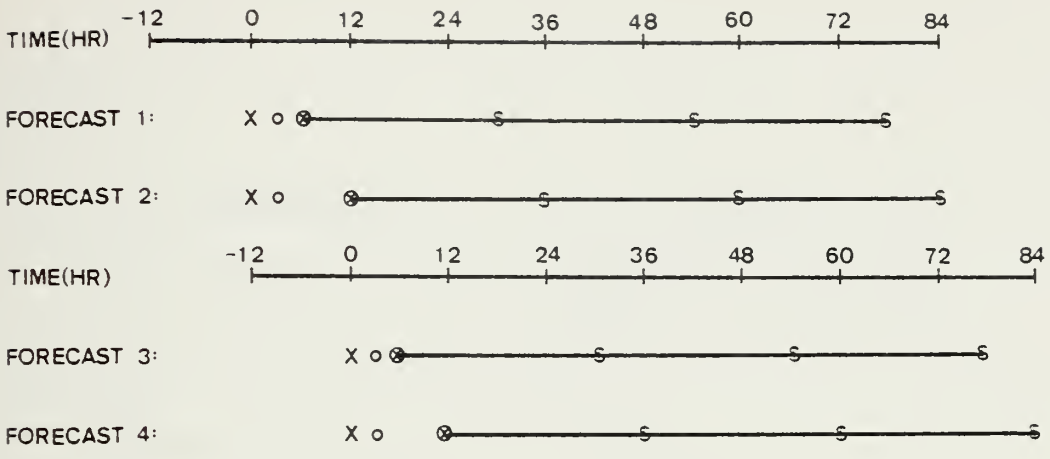

Figure 2. The forecasts 1, 2, 3 and 4 represent the 4 scheduled warnings issued by JTWC each day. The X marks upper level analysis time; o represents time that forecasts would be available from this research, * represents the time warnings are issued; and $ represents warning forecast times. This diagram illustrates the reason for the 30, 36-, 54-, 60-, 78- and 84-hour forecast intervals.

TABLE I

Number of cases available per forecast time interval

Forecast Interval	Number of Cases
30	504
36	482
54	387
60	360
78	273
80	250

much faster than the tropical storm and the synoptic features south of the storm.

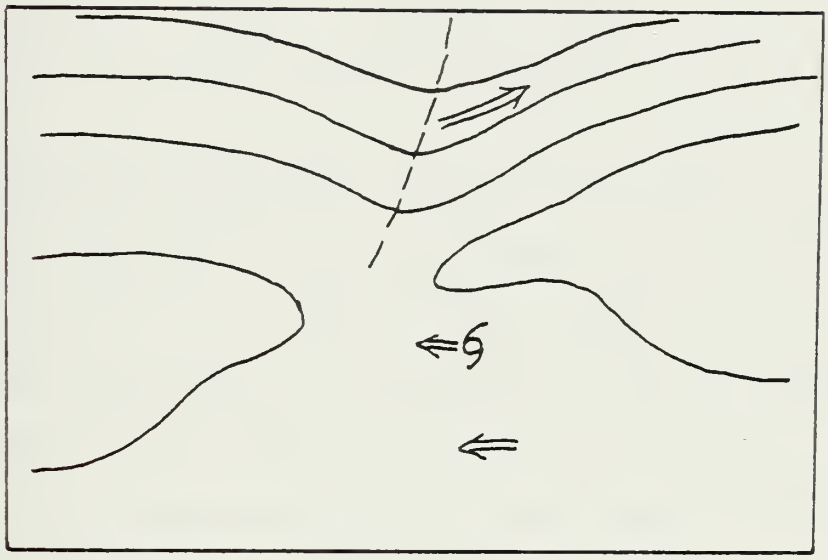

Figure 3. This is a very generalized picture of the flow as it appears on the grid. Note the difference in speed, relative to the storm, of features to the north of the storm compared to features south of the storm.

B. DATA NORMALIZATION

Having interpolated the data to the 120 standardized grid points for each of the 504 maps, the data must be arranged into a matrix for the EOF analysis. Each column represents a map type and each row represents a grid point. The result is a 120 x 504 matrix. The data must be

normalized at each point to use the EOF method of extracting "signal" from "noise". This "noise" comes primarily from errors in the observations used to construct the D-value fields and from subgrid scale phenomena. The normalization, performed by rows, is

$$X_{ij} = \frac{x_{ij} - \bar{x}_j}{s_j} \qquad (2.1)$$

where i represents the map number; j represents the grid point; X_{ij} represents the standardized D-value, $\bar{x}_j$ represents the mean (over i) of the grid-point values j; s_j represents the standard deviation at grid-point j; and x_{ij} represents the D-values of the ith map at grid-point j.

Two other normalization procedures were tried: 1) normalizing each map (i.e. column), using $\bar{x}_i$ and s_i and 2) normalizing over the whole matrix using $\bar{x}$ and s, as constants. Each method emphasized certain aspects of the data field at the expense of another. Fig. 4 and Fig. 5 are examples of the results of the different normalizing schemes after the EOF computations and truncation. Normalization by grid point (as in (2.1)) insures that the variance at each grid point is given equal weight and emphasizes the features in the southern portion of the maps. Normalization by map insures that the variance of each map is given equal weight. Since most of the variance, within each map, is usually in the

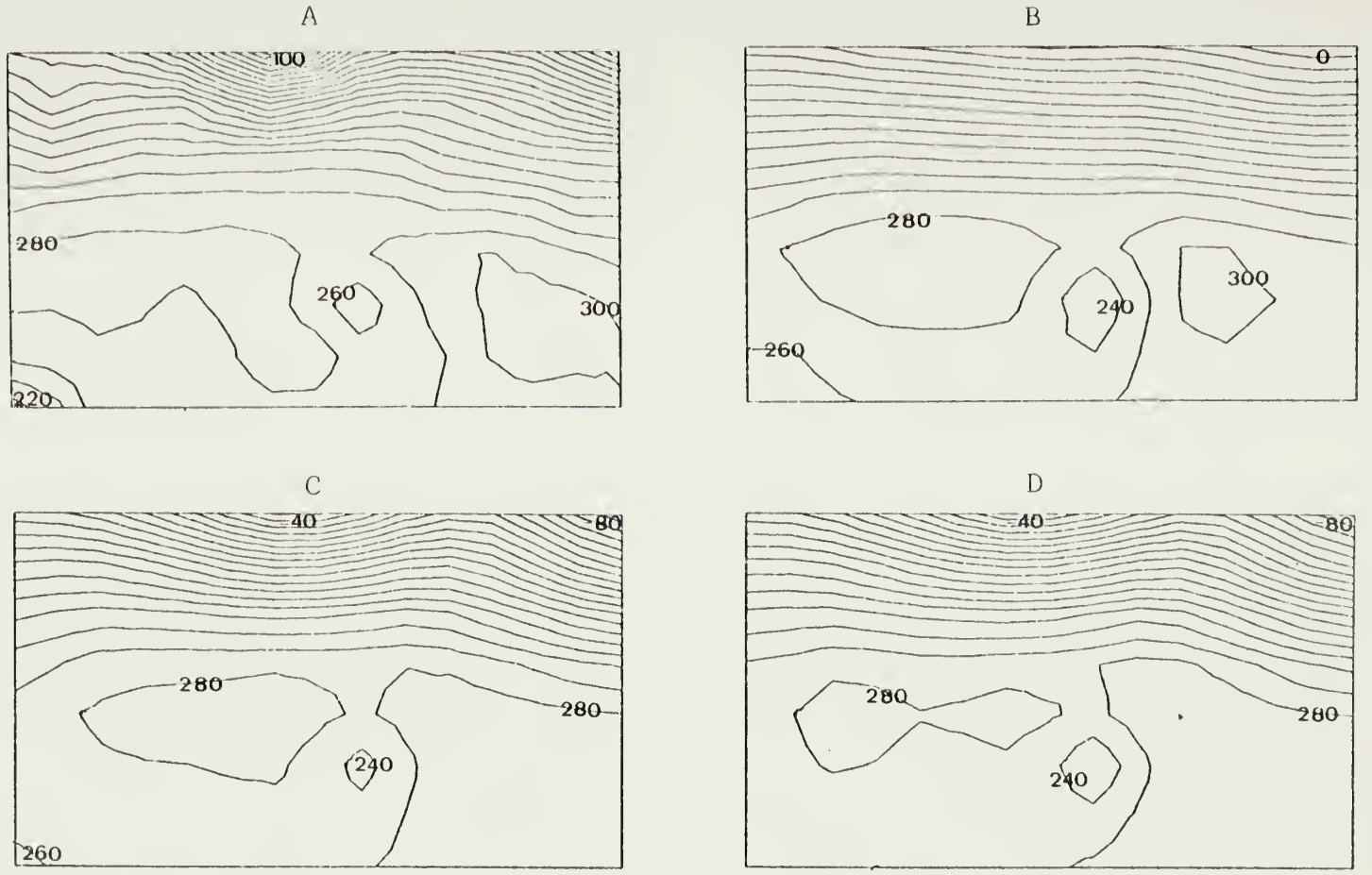

Figure 4. The effect of the different normalization schemes at 500 mb. The four representations are for 00 GMT, 18 Mar 1967. A is the actual field; B, C and D are the EOF representations (truncated at 10 terms) using grid-point normalization, whole field normalization and map normalization, respectively. The isopleths are D-values (m).

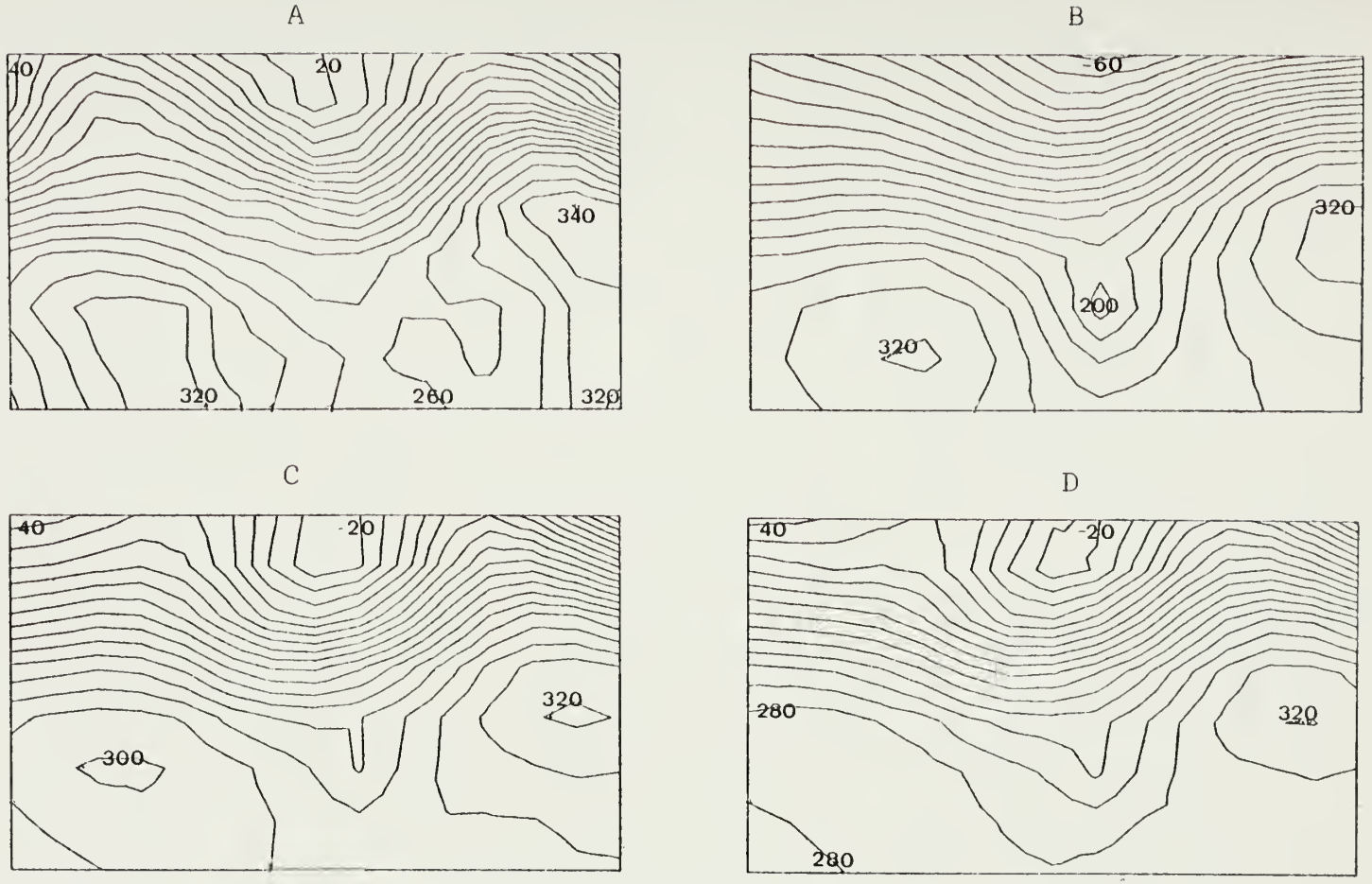

Figure 5. Similar to Fig. 4 except for 12 GMT 25 Aug 1967.

northern region, this method generally emphasizes the northern regions, but not always. Normalization by the entire field insures that the variance of each point of each map is given equal weight. The effect of this method varies from map to map and depends on how the variance of the map is distributed relative to the average variance over all cases.

In Fig. 4A and Fig. 5A, the actual map data, first note the detail and then the "noise" in the grids, primarily represented by the unsmoothed isopleths. Then note how much smoother the truncated eigenvector fields are regardless of the normalization scheme. In Fig. 4B and Fig. 5B, the grid-point normalized maps, the definition and strength of the troughs in the westerlies in the northern portions of the grid are poor. However, the tropical sections of the grid are represented well. Particularly note the low pressure in the southwest corner of Fig. 5B that was poorly analyzed in both Fig. 5C and Fig. 5D. The maps normalized by the entire map's mean and standard deviation, Fig. 4C and Fig. 5C, have good representations of troughs in the westerlies. However, they miss the intensity of the low pressure area in the southwest section of Fig. 5C. Almost the same comments can be made for Fig. 4D and Fig. 5D as for Fig. 4C and Fig. 5C. The method of normalization by grid points used here (eqn. (2.1)) was selected to keep the large variance in the northern part of the grid from overpowering the variance in the

southern part. Also by following this method, follow-on studies will be able to use the Preisendorfer and Barnett (1977) method for truncating the EOF series. In Fig. 6, the maps of the 850, 700 and 500 mb grid-point means and standard deviations, that are used to normalize the grid via (2.1), are presented. Particularly note the north-south variations of the means and the large standard deviations in the northern portions of the maps at all levels. There is also a relative maximum in the standard deviations at the location of the tropical cyclone, which indicates a sizable variation in storm intensity from map to map.

C. EMPIRICAL ORTHOGONAL FUNCTION (EOF) ANALYSIS

The concept of using EOF analysis in meteorology was first introduced by Lorenz (1956). His description formed the basis for a wide range of uses of the technique in the meteorological field. Kutzbach (1967) provides a concise mathematical and descriptive outline of the technique upon which this research is based. The object of using the EOF technique is two-fold. First, it is used in an attempt to separate the true "signal" from random "noise" in the D-value fields. Secondly, it provides a method to reduce the number of variables from a large number of highly correlated variables to a smaller number of independent variables. Only a general description of the concept and procedure is

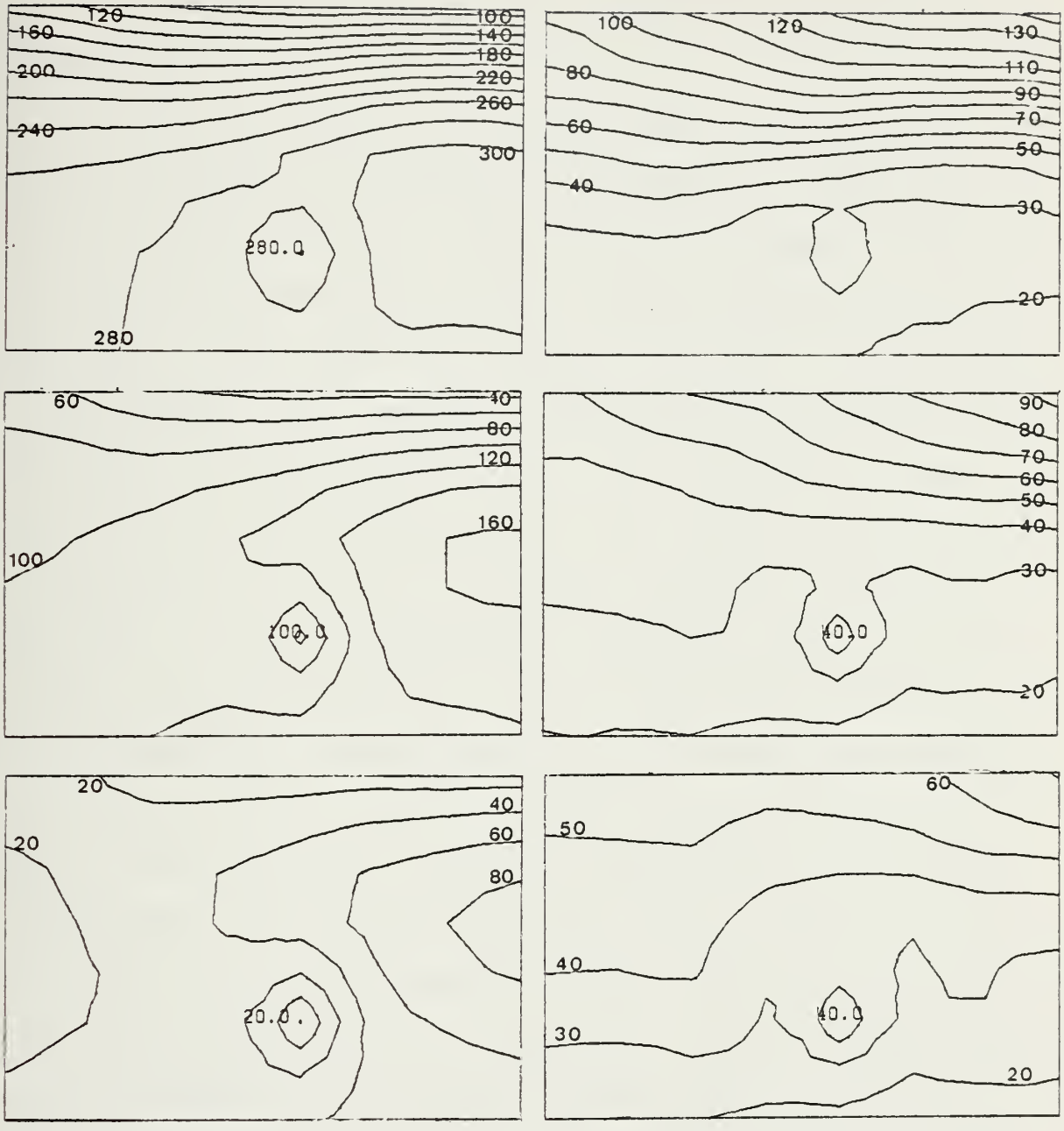

Figure 6. The D-value means (left side) and standard deviations (right side) for 850 mb (bottom), 700 mb (middle) and 500 mb (top). The isopleths are D-values (m).

included here. A more detailed mathematical description of the process is presented in Appendix A. A listing of the computer subroutines used in the analysis is given in Appendix B.

A 120 x 504 matrix X was formed, such that each grid point in each map is normalized in relation to that grid point over the 504 maps. Each map may be thought of as a vector in 120-dimensional space. The 504 vectors representing each map will tend to be highly correlated. Therefore, it is expected that the points representing the position of the head of the 504 vectors will tend to cluster in space. The objective of the EOF analysis is to use the 504 points to determine a set of 120 orthogonal vectors to represent the basis of the 120-dimensional orthogonal space. To determine this 120-dimensional space, first form the symmetric normalized covariance matrix. The columns are vectors representing the variance in the data matrix. The first axis in this new space, hereafter referred to as the first eigenvector, will be determined such that it will be a linear best fit to the variance vectors. This procedure is equivalent to maximizing the explained variance (eigenvalue) and minimizing the unexplained variance (residual) of the data by the first eigenvector. The second eigenvector will again be a linear best fit to the variance vectors, with the additional requirement that it be orthogonal to the first.

Thus, this eigenvector will explain as much of the remaining variance as possible. The third eigenvector will again be the linear best fit to the variance vector, but it must now be orthogonal to the first two eigenvectors. The procedure will be continued until all the variance is explained, which will be equivalent to having an eigenvector for each of the 120 dimensions.

One may think of EOF analysis as being analogous to a Fourier series. Instead of representing the data as a linear combination of space-orthogonal sines and cosines, the space-orthogonal functions in the EOF analysis are derived from the actual variance in the data. As with Fourier analysis, each eigenvector has an associated (time) coefficient. This coefficient, when combined with its eigenfunction and summed over the entire eigenspace, provides an exact reproduction of the original field. That is,

$$X(x,t) = \sum_{m=1}^{M} EOF_m(x)\, C_m(t) \qquad (2.2)$$

where X represents the value at grid-point x of map t in the data matrix; EOF_m represents the empirical orthogonal functions which are derived by relating the unit eigenvectors to the original 120-dimensional space; and C_m are the time

coefficients (in this case time is determined by the different map times) related to the m th eigenvalue, and M = 120. These coefficients are time orthogonal (Kutzbach, 1967) and are obtained from the eigenvectors and the original data field. The specific mathematical relationships are described in Appendix A. When a linear combination of eigenvectors and their respective time coefficients are translated into the original space, the eigenvectors represent a series of functions in the same manner as sines and cosines represent functions in Fourier analysis. A truncated linear combination (i.e. (2.2) with M less than 120) can be shown to approximate the original maps with the "noise" removed (Preisendorfer and Barnett, 1977).

Upon completion of the EOF analysis, the eigenvectors and eigenvalues represent solutions to the maximization of an "explained variance" problem. Thus, depending on the geophysical parameter being analyzed and the quality of the data available, the first few eigenvectors often represent a large fraction of the variance in the data set. Preisendorfer and Barnett (1977) have developed an empirical formula for separation of true "signal" from "noise" in EOF analysis. Since each eigenvector represents a weighted portion of the variance, this separation can be accomplished by truncating the number of eigenvectors included in the EOF. Because of time constraints for this study, an arbitrary truncation was made at eigenvector 10. Without formal

application of the Preisendorfer-Barnett techniques, we can not be assured of the statistical significance of the higher order eigenvalues. This is one aspect that needs to be optimized in any subsequent studies.

Because most of the variance is contained in the first few eigenvectors, excellent "noise-free" representations can be made from just a few of them. The cumulative percent of the variance expressed by the linear combination of eigenvectors derived from the 504 case studies is shown in Table II. For example, 83-85 percent of the variability is expressed in the first 10 eigenvectors at all three levels. In fact, beyond a certain point, the eigenvectors represent such a small portion of the variance that they just represent noise in the map fields. In this manner we can reduce the number of variables required to represent the maps from 120 grid points to 10 coefficients of the orthogonal eigenvectors. In the next section, we use these 10 coefficients ($C_m(t)$) to derive a series of characteristic maps which we will call map types.

The maps in Fig. 7 represent case number 1 and are an example of how the linear combinations of the EOF build the map. The last map in Fig. 7 is the same as shown in Fig. 4A. Without describing in detail each map in Fig. 7, it can be seen that the more drastic changes in the pattern occur in the belt of westerlies after the inclusion of more than 10

TABLE II

Cumulative percent of variance and the actual variance (m^2) or eigenvalue as expressed by the linear combination of eigenvectors for each level. An arbitrary cutoff at 10 eigenvectors was used here.

Eigen vector	850 mb		700 mb		500 mb	
	Percent	Variance	Percent	Variance	Percent	Variance
1	34	40.15	25	29.53	33	39.38
2	51	20.35	46	25.95	51	21.61
3	60	11.09	56	11.17	59	9.32
4	67	8.42	62	7.91	65	7.45
5	72	6.09	68	7.11	70	6.05
6	75	4.14	72	5.14	75	5.29
7	78	3.42	76	3.77	78	3.98
8	81	2.94	79	3.59	81	3.11
9	83	2.56	81	2.57	83	2.49
10	85	2.16	83	2.29	85	2.11
11	86	1.74	84	1.98	86	1.86
12	87	1.52	86	1.61	88	1.71
13	88	1.28	88	1.41	89	1.41
14	89	1.05	89	1.25	90	1.19
15	90	.95	90	1.13	91	1.05
16	91	.89	91	1.06	91	.95
17	92	.84	91	.97	92	.78
18	92	.65	92	.74	93	.77
19	93	.57	92	.62	93	.69
20	93	.55	92	.61	94	.58
.	.		.		.	
.	.		.		.	
.	.		.		.	
120	100		100		100	

to 15 terms. With just one term, the basic flow is established - moderate westerlies, weak gradient in the tropics and a trough where the storm is located. After including about 15 terms only slight refinements of the pattern take place. The "noise" in the map starts to become more obvious with the inclusion of 40 terms. The isopleths begin to show irregularities and are not as smooth as in the earlier maps. Beyond 80 terms it is almost impossible to see any differences.

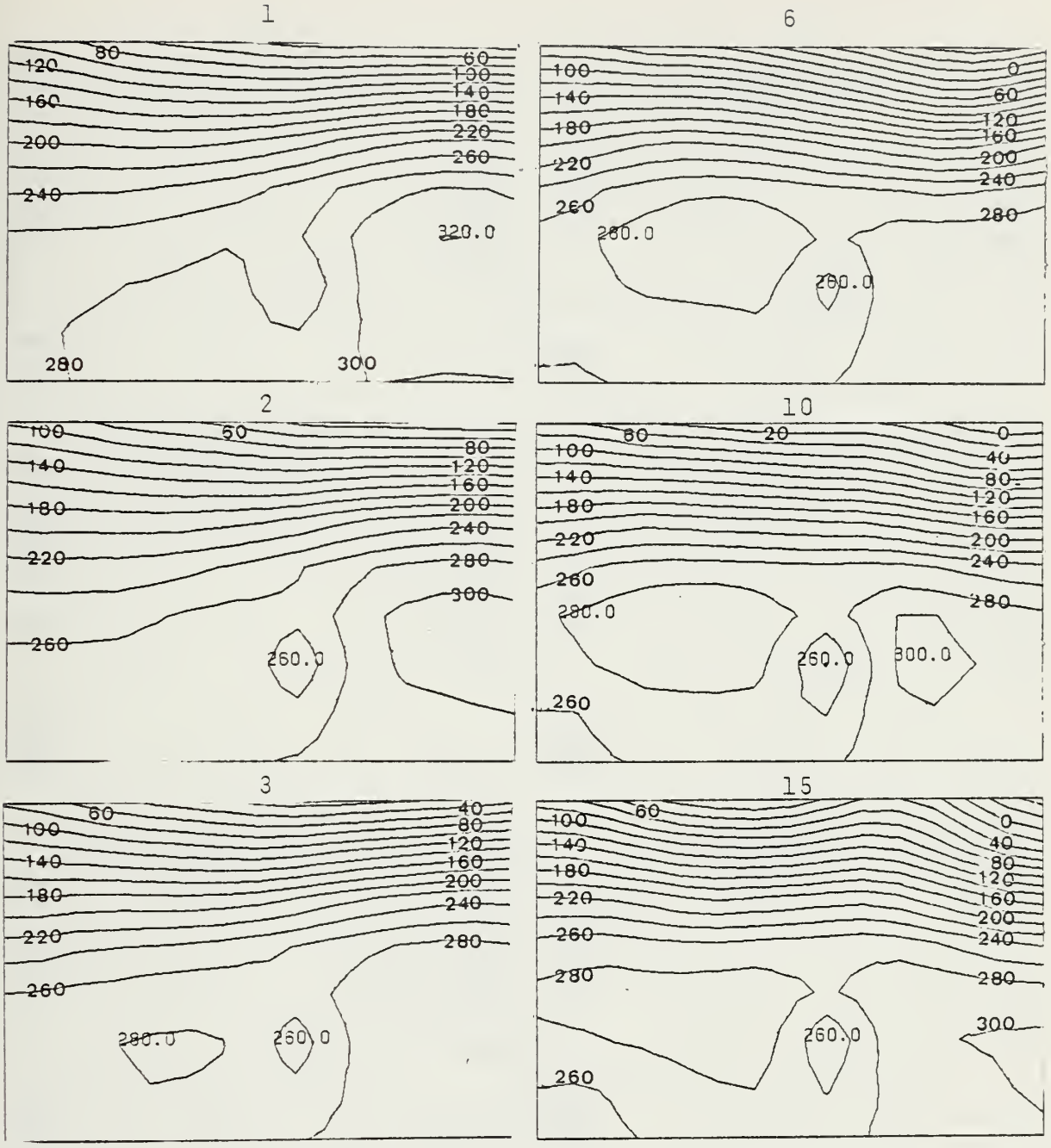

Figure 7. An example of the effect of truncation of the EOF for 00 GMT, 18 Mar 1967. The number above the map is the number of terms included (the truncation point). The isopleths are D-values (m).

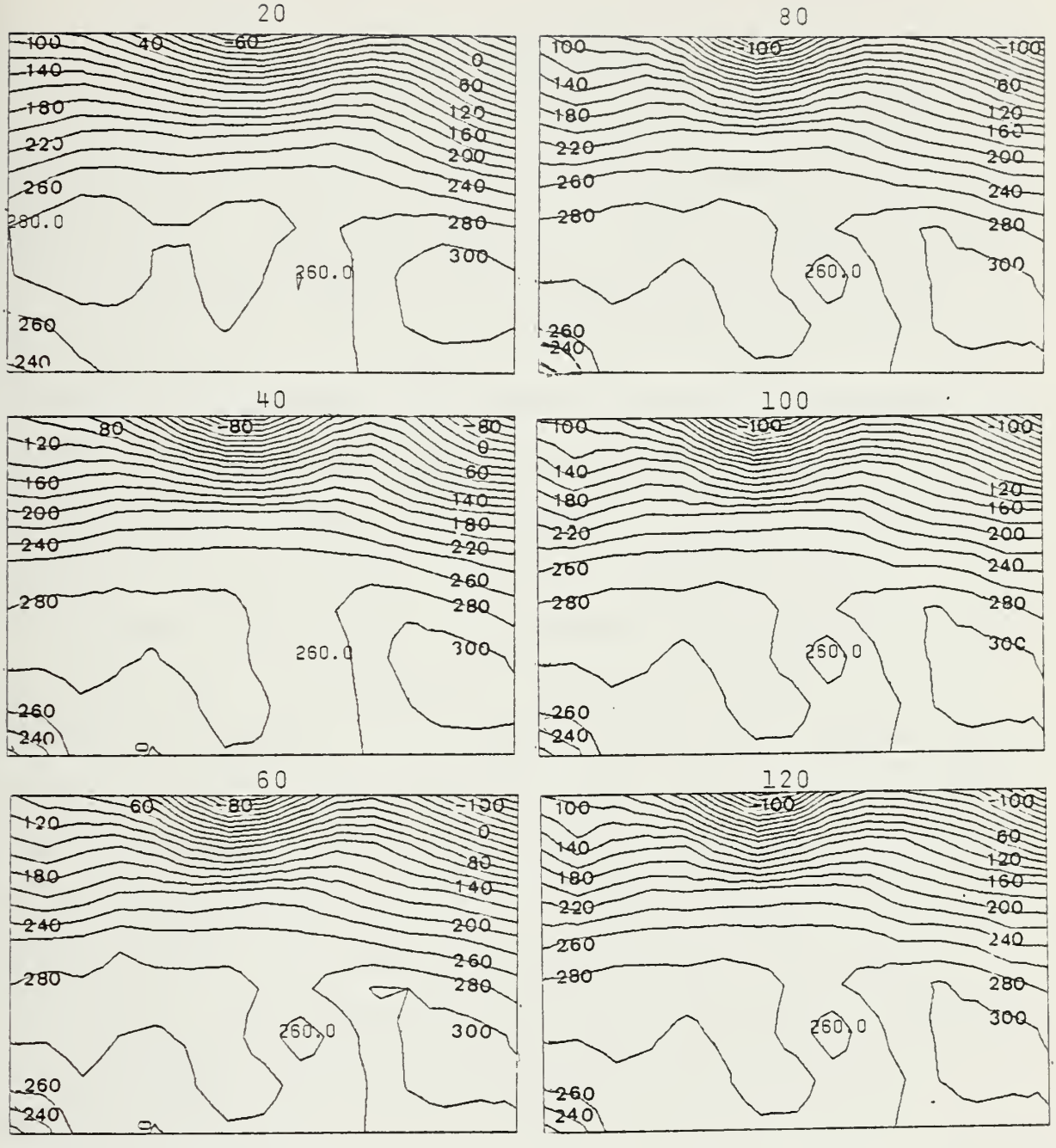

Figure 7. continued

III. MAP TYPING

At this point, three choices are available. The EOF analysis could be treated just as an approximate method to eliminate the noise from the data. Then "noise-free" maps could be produced and map typed exactly as in Lund (1963). The second choice, and the one followed here, was to use the truncated EOF analysis to compare the maps in eigenvector space. The actual map typing procedure is similar to the Lund procedure, except that instead of having 120 variables, there are only 10 in the truncated eigenvector space.

A third possibility is to consider the eigenvectors as the map types. The grid-point normalized fields could be compared in either a least squares approach or a direct correlation approach, to the actual eigenvectors. This method was not chosen in this study since the statistical significance of each eigenvector was not known (Preisendorfer and Barnett, 1977). By using the coefficients, and therefore essentially the approximated data sets, we hoped to minimize the problem of not knowing the statistically derived truncation point.

As described previously, the eigenvectors represent the axes in space. It is the coefficients that actually locate the position of each individual map in that space. Although

each map is an independent sample, the maps are highly correlated and will when plotted in space tend to form clusters. The idea is to find the map that is most representative of each cluster and call that the map type. To do this, each map is compared in the least squares sense to all the other maps. This is done by using the coefficients of the truncated eigenvector space in the following manner

$$LS_{jk} = \sum_{i=1}^{10} (C_{ij} - C_{ik})^2 / s_i^2$$

where LS_{jk} is the least squares value comparing map j with map k; C_{ij} is the coefficient of the ith eigenvector of map j; C_{ik} is the coefficient of the ith eigenvector of map k; and s_i^2 is the variance accounted for by the ith eigenvector in the truncated eigenvector set. The LS_{jk} value for each map with all other maps is computed and stored.

Now, search for the map that is most representative of the "tightest" cluster and designate this as map type 1. To do this, the map that had the largest number of other maps falling within the least squares radius of five units was designated map type 1. The least squares radius of five units was selected arbitrarily on the basis of a trial and error method. Since map type 1 was the most common map, it should have the largest number of maps associated with it, but no so many that the sample is so depleted that the

other map types can not be determined. The least squares radius of five units appeared to give the most representative sets. It is possible that a more rigorous approach for finding a statistically valid value of the cluster radius could be determined.

Type 1 and all maps selected within the least squares radius of five were removed from the sample prior to the selection of the next map type. Since it is anticipated that the next cluster would not be as tight as the first, the least squares radius was increased by two units. Map type 2 is then selected as the map with the largest number of remaining maps within a least squares radius of seven units. Then map type 2 and all maps within seven units of it were removed from the sample. The process, with an increasingly larger radius, is continued until at least 470 maps were selected.

Finally, all the remaining maps are lumped together in the last type. The actual map type is selected in the same manner as all the others, except that now all the remaining maps are placed with this type regardless of the value of the least squares radius.

When this process was completed, there were 11 or 12 map types for each level, each with a number of other maps similar to it. As the typing process evolved, there was no attempt to keep the least square radius circles from overlapping. Thus, the map typing is not complete, because a map in type 1 may actually be closer to map type 3 than it

is to map type 1. Therefore, each map must again be compared, in the least squares sense, to each of the selected, most representative map types. Then each map is grouped with the type it is nearest to in space. Now the map typing is complete. Only the results of the 500 mb map typing are discussed here. Similar comments could be made for the 850 and 700 mb map types, but in the interest of brevity just the map types and forecast results are presented in Appendix C.

Each of the eleven 500 mb map types in Fig. 8 is clearly different. The following is a discussion of the distinguishing synoptic features for each map type:

Map Type 1: The storm is situated moderately deep in the tropics. To the west of the storm the pressure gradient is very weak. The broad ridge to the east of the storm is also weak. Well to the north of the storm the pressure gradient of the westerlies is weak with troughing indicated to the north-northwest of the storm at a distance of approximately 700 n.mi.

Map Type 2: Here the storm is deep in the tropical belt with a strong east-west subtropical ridge centered approximately 600 n.mi. almost due north of the storm. A weak extension of this ridge separates the storm from the broad low 1800 n.mi. to the west of the storm. To the east of the storm the influence of the strong subtropical ridge extends to the southern boundary of the map.

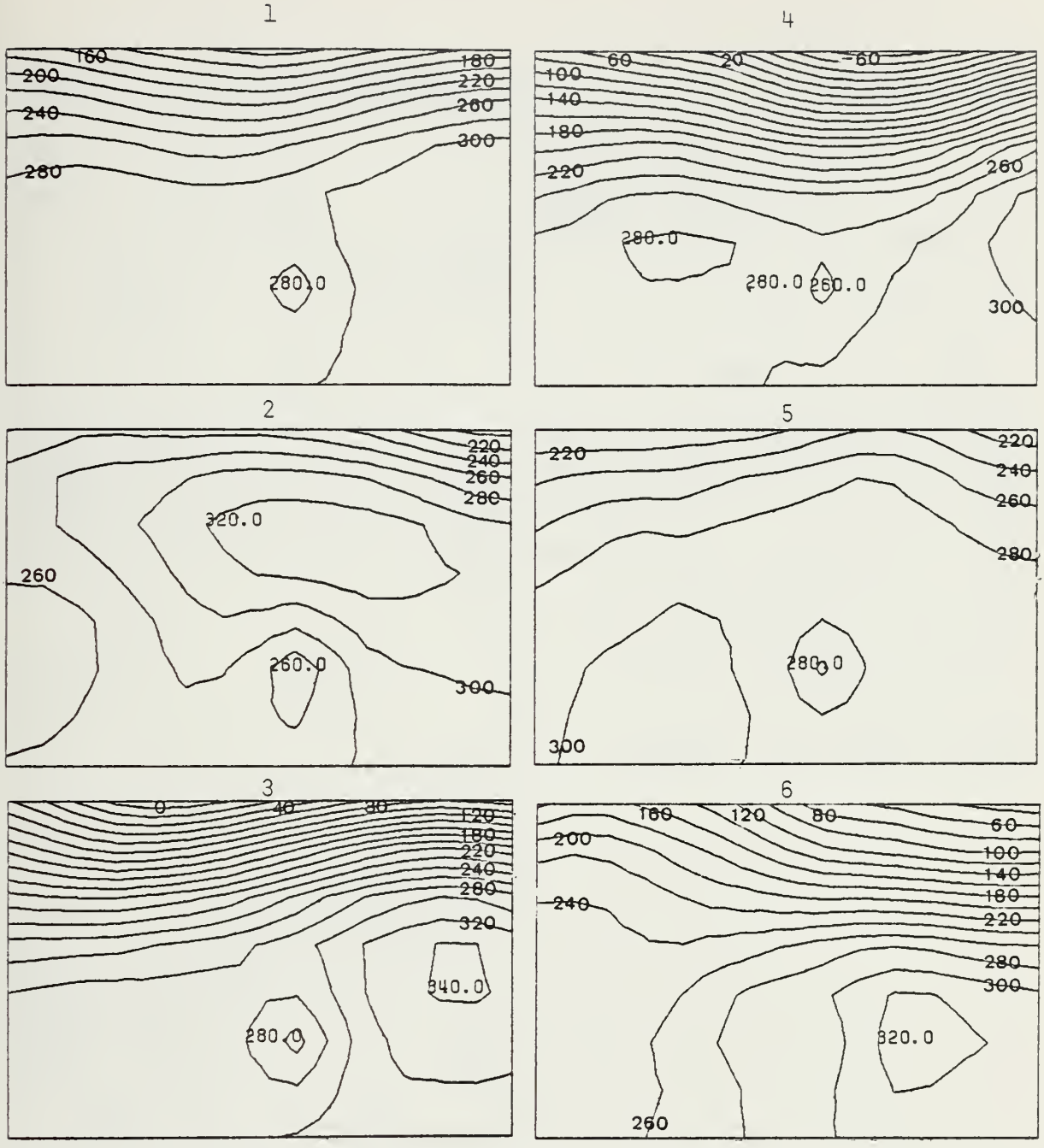

Figure 8. The 500 mb map types. The number above each map refers to the map type number, i.e. in the order selected. Isopleths are D-values (m).

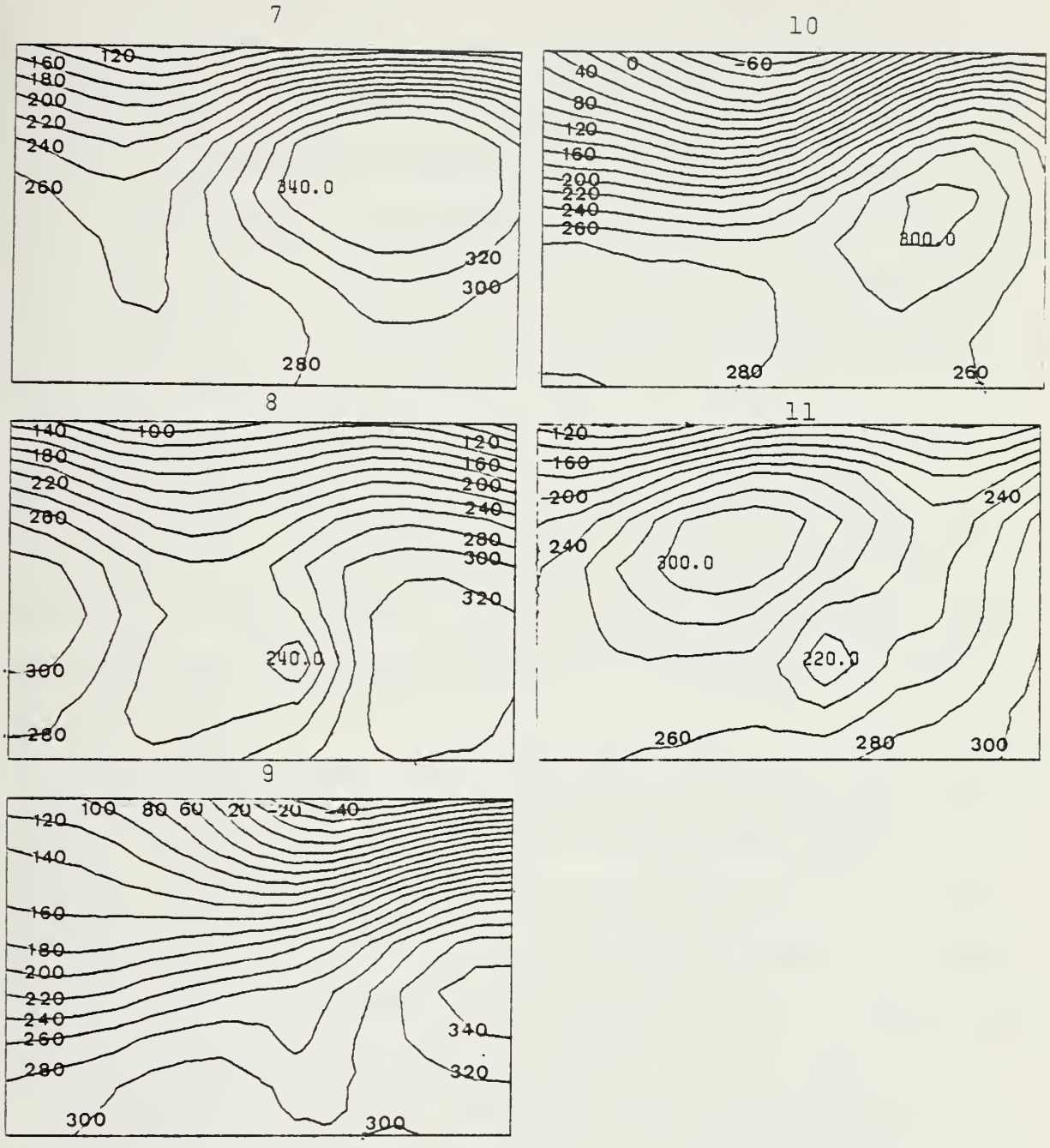

Figure 8. continued

Map Type 3: In this case the storm is near the northern boundary of the tropical region, with weak pressure gradients to the west and west-southwest. The center of a strong cell at the eastern extremity of the subtropical ridge is evident approximately 1200 n.mi. to the east-northeast of the storm. The strong westerlies that begin only 600-700 n.mi. to the north of the storm further intensity to the north of this ridge cell. There is a weak trough to the west-northwest.

Map Type 4: Here the storm is only 300-400 n.mi. from the strong westerlies. It is located between two cells of the subtropical ridge with the stronger cell due east at the edge of the grid. There is a trough in the westerlies almost due north with the storm apparently at the southern extent of the trough.

Map Type 5: Again the storm appears to be located deep in the tropics because of the surrounding weak pressure gradient and the absence of the strong westerly flow in the northern portions of the grid. There is a broad weak ridge to the east of the storm. An extension of this ridge can be seen in the westerlies far to the north of the storm.

Map Type 6: In this case the presence of the storm is barely discernable. The implication is that the storm is either very weak or that its influence is not seen at 500 mb. Another point that needs to be made here is that the data on the standard grids is interpolated directly from the

analysis fields as they appear on the FNOC data tape. Some fields may have the storm location and intensity inserted manually while others may not. In the scope of this research, there is no way of knowing whether or not the bogus data were applied to any particular map used in our data set. The center of the subtropical ridge is positioned only about 500 n.mi. to the east of the storm with its influence extending well to the west of the storm. The westerlies to the north are of only moderate intensity with a trough-ridge pattern in the northwest quarter of the grid.

Map Type 7: Again the storm circulation is only weakly apparent at 500 mb by the slight deformation in the southwest section of a strong subtropical ridge to the northeast of the storm. In this case however, there is a strong mid-latitude trough system extending to the latitude of the storm to the storm's west. The westerlies through the trough are moderate, increasing in speed north of the subtropical ridge position.

Map Type 8: In this case the storm's influence is felt strongly at 500 mb. The D-value at the storm's location is less than 240 m, which is more intense than all other map types except map type 11. The storm is located between two strong cells in the subtropical ridge. The pressure gradient to the east of the storm is much steeper than to the west within 600 n.mi. of the storm. The westerlies appear to be of moderate intensity with a well defined trough to the north-northwest.

Map Type 9: All indications here are that the storm, as represented by the trough in the westerlies, has almost entirely departed the tropics. In the western portion of the grid the subtropical ridge has either completely broken down or the storm is so far north that the western part of the ridge is south of the grid. The ridge center to the east of the storm is strong, and there is a strong westerly current to the north of it. There is a trough in the westerlies almost due north of the storm.

Map Type 10: As with map types 6 and 7, the storm here is barely discernable at 500 mb. It appears here as a break in the ridge. The ridge axis is oriented from east-northeast of the storm to almost due west of the storm and is much stronger in the northeastern extension. The westerlies are strong with a trough located north-northwest of the storm.

Map Type 11: In this case the storm appears deeper than in all the others. The storm appears to be 700-800 n.mi. south of the subtropical ridge axis. A strong cell in the ridge is evident to the northwest of the storm. A mid-latitude trough is evident in the northeast corner of the grid, and a trough extends through a weakness in the ridge to the storm. The westerly flow is well removed from the storm (1100-1200 n.mi.).

With this brief discussion of each map, it is clear that each represents a different synoptic situation. Fig. 9 and Fig. 10 show examples of map types 1 and 2 storm cases from

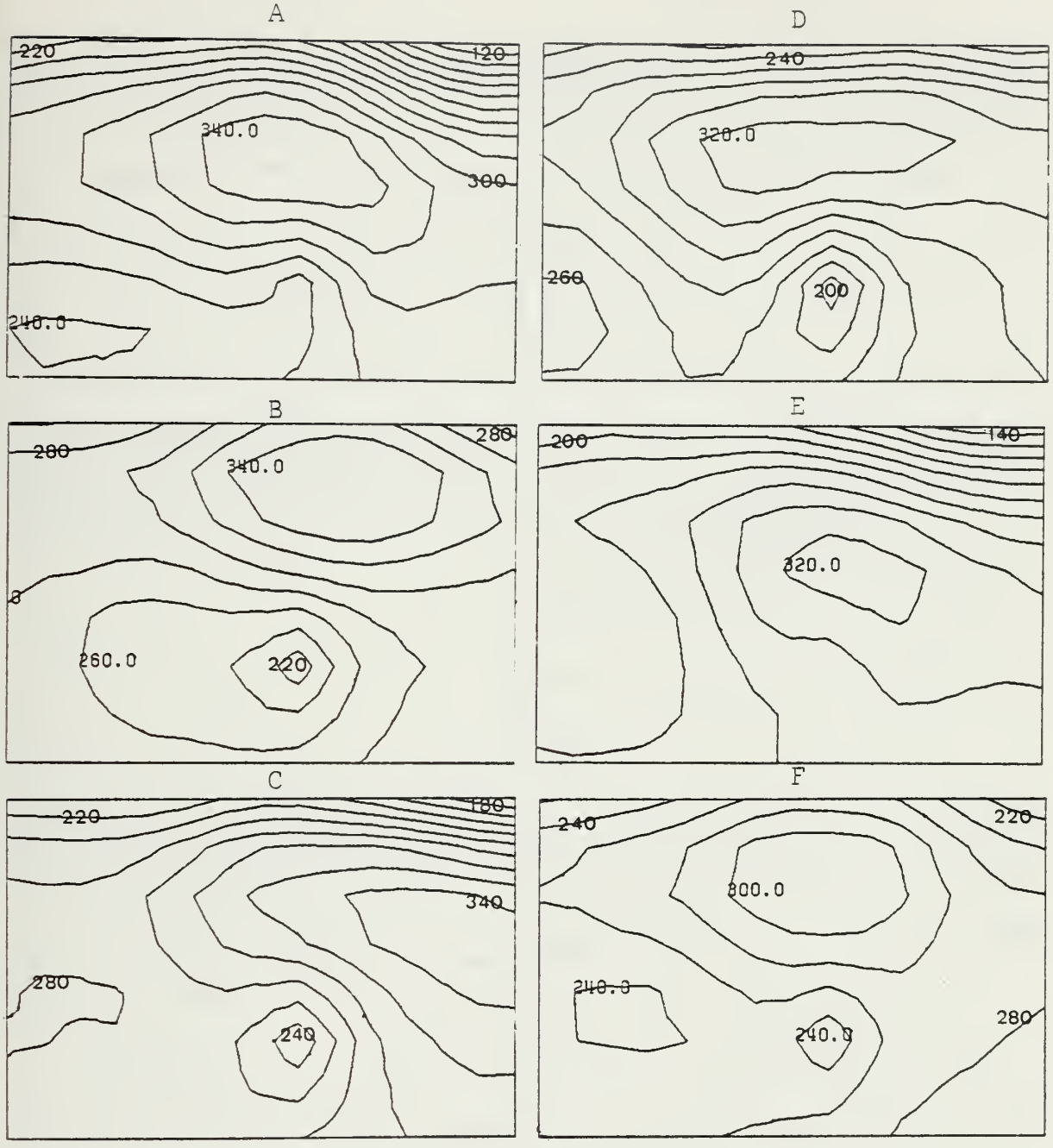

Figure 9. Examples of map type 2 (500 mb). The letters above the maps are for reference for the text. The isopleths are D-values (m).

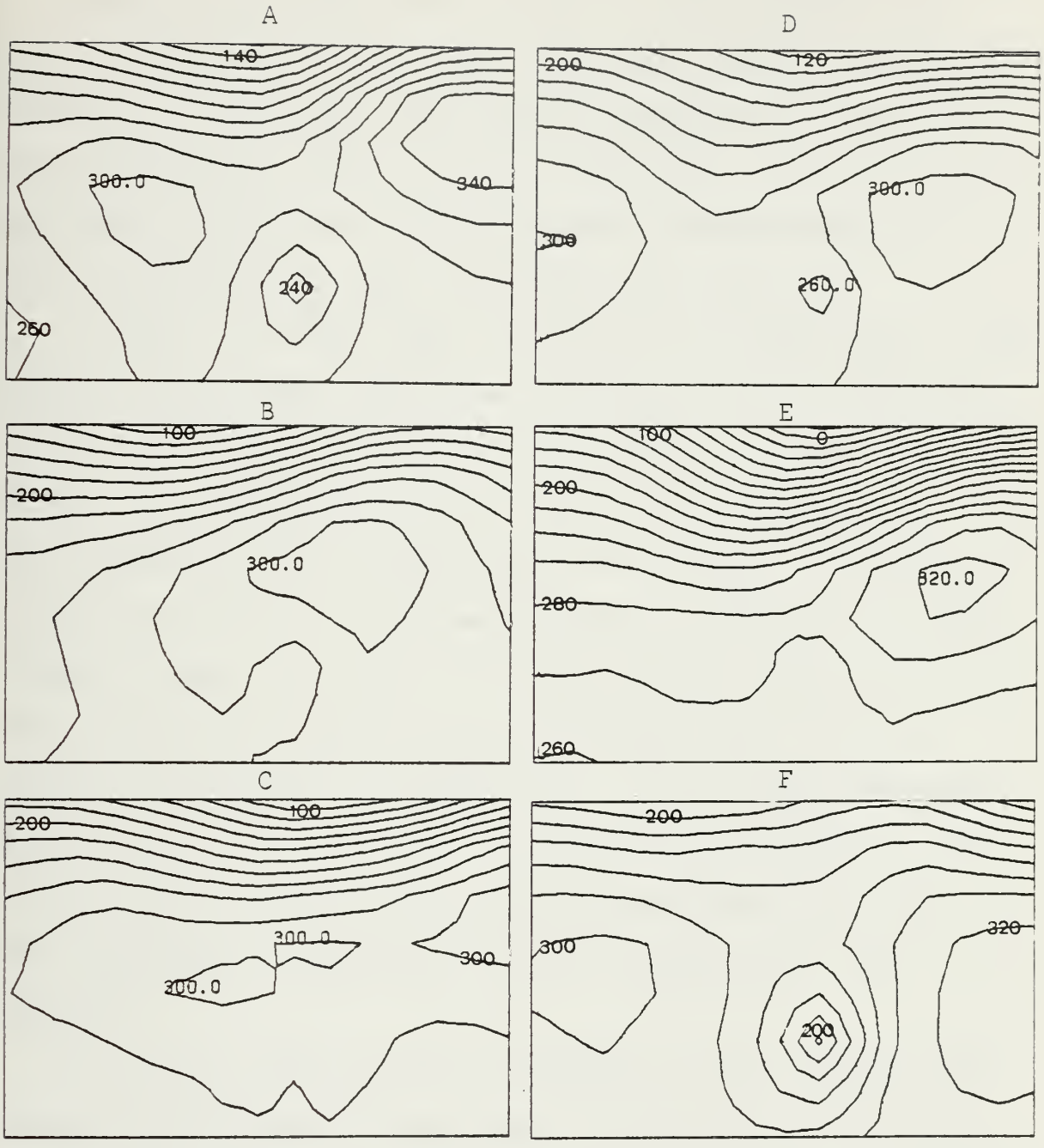

Figure 10. Examples of map type 1 (500 mb). The letters above the maps are for reference for the text. The isopleths are D-values (m).

the sample (more examples of the other map types are shown in Appendix D). Since each map had to be classified with one of the characteristic maps, the least squared distances between the individual maps and its characteristic map may vary considerably even within one map type. Thus, it is to be expected that some maps show greater similarities to their characteristic map than others (see Fig. 8).

In Fig. 9, the map type 2 maps have a strong ridge to the north of the storm. The actual position of the primary cell varies from north-northwest of the storm to northeast of the storm. All the maps show the storm deep in the tropics. The intensity of the storm varies considerably. In Fig. 9, A and E, the storm is very weak at 500 mb, while it is very strong in Fig. 9, B and D. The westerlies, well to the north, vary in intensity but are generally fairly weak and the pattern is similar to the map type. All the cases indicate a broad area of low pressure in the tropics due west of the storm, except in Fig. 9C when the low pressure is to the west-southwest. Therefore the basic patterns are very similar.

In Fig. 10, the map type 1 examples do not show as much similarity to their map type case as do the map type 2 examples, but the basic patterns are still evident. All maps show strong evidence of the trough in the westerlies to the north-northwest of the storm that is found in the characteristic map. All cases show westerlies that are weak to

moderate in intensity. The storm is always moderately deep in the tropics with the exception of Fig. 10E. In Fig. 10, B, C, D, and E, the storm is weakly represented at 500 mb as in the map type storm. All show the ridge basically to the east of the storm. Again, it is not too difficult to see the similarities.

After examining Fig. 7 and noting that map type number 1 may have needed more terms to adequately define the details of the synoptic features, one actual size (500 mb) with the EOF series truncated at 20 terms (approximately 93 percent of the variance) was tried. The map types selected using the 20 EOF terms are shown in Fig. 11. The selection procedure was similar to that described above except that a larger (15 versus 5) initial least squares distance was required initially in determining the characteristic map types. The inclusion of more terms appears to better separate the maps in eigenvector space. The maps have considerably more detail and the D-values in the troughs and ridges much more closely resemble the actual maps. It is clear that the map typing is very sensitive to the number of EOF modes that are retained in the analysis. It is possible that 10 EOF terms may not be sufficient to properly represent the significant features for several possible reasons. First the data should have already been somewhat filtered, since the FNOC fields have been objectively analyzed. Because the grid size

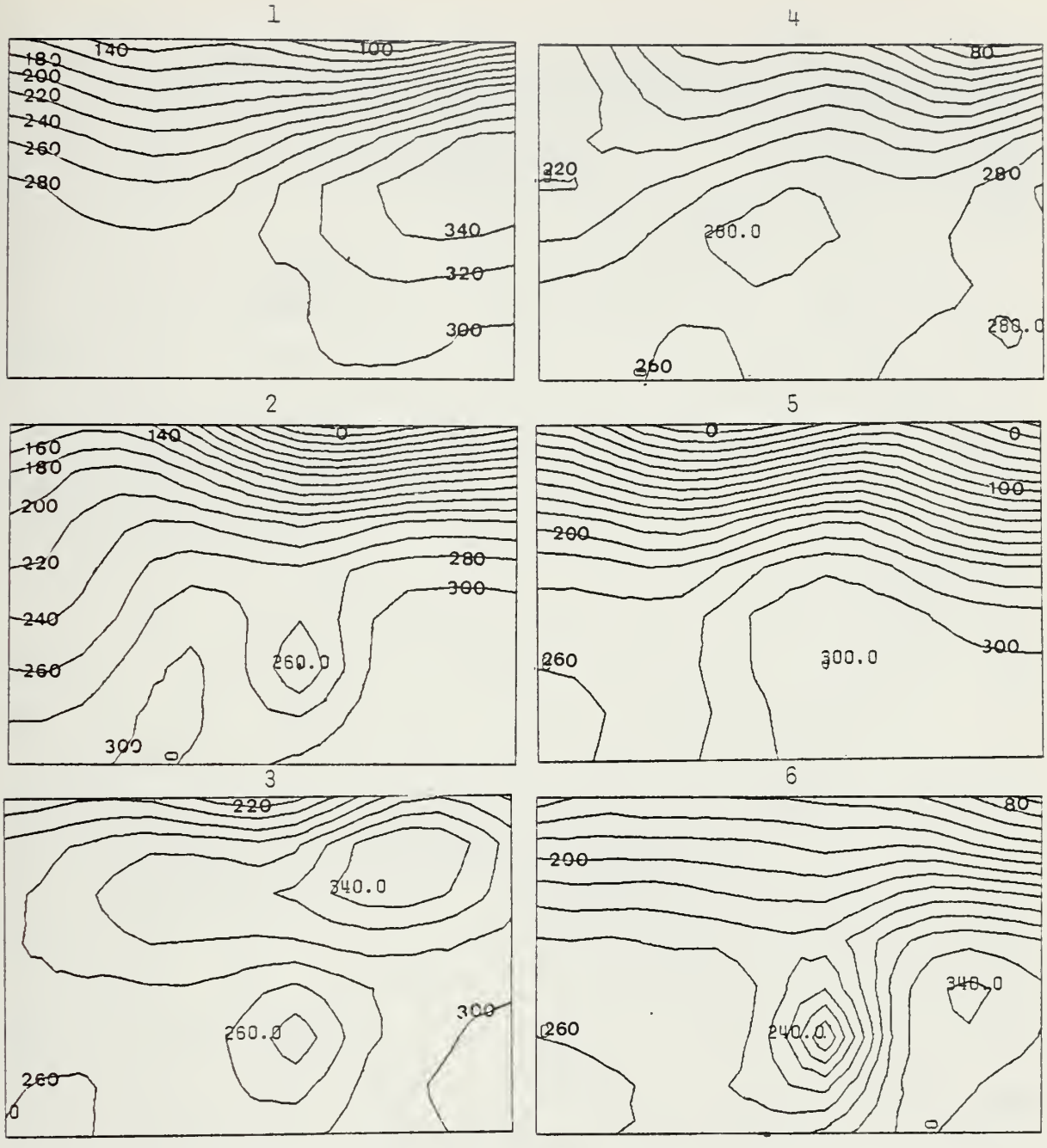

Figure 11. The 500 mb map types using 20 terms of the EOF. The number above the maps refer to the map type number. The isopleths are D-values (m).

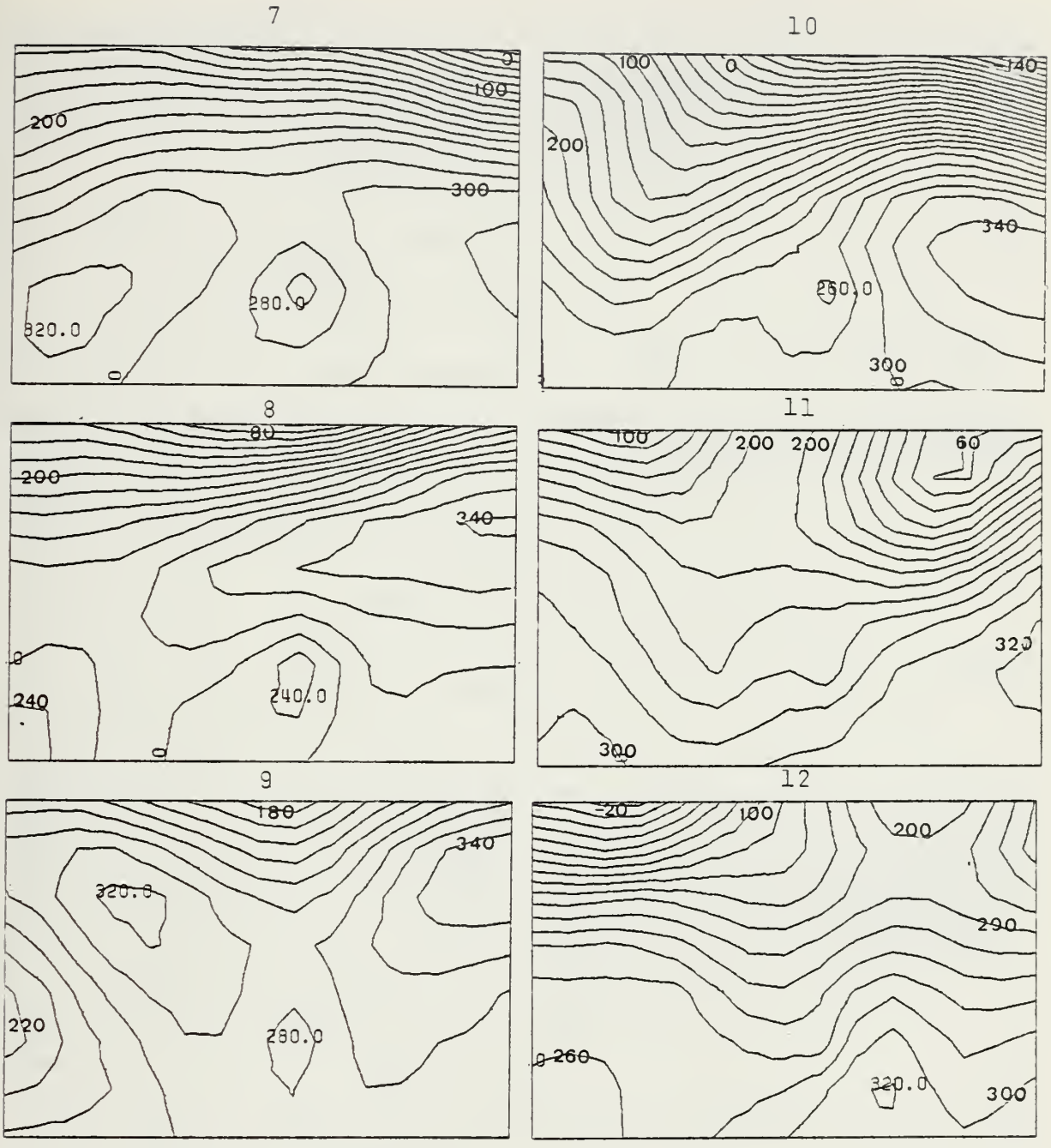

Figure 11. continued

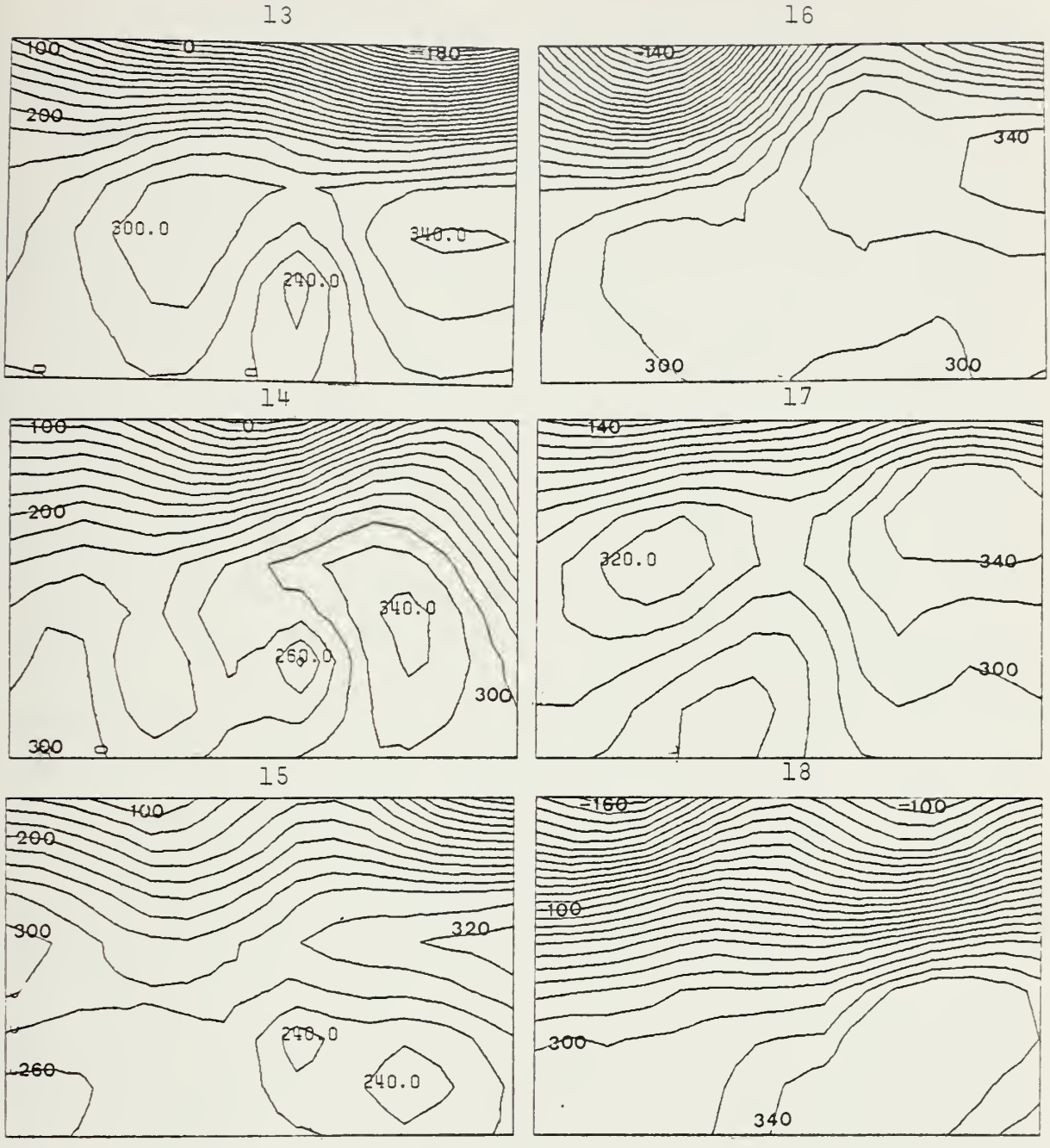

Figure 11. continued

used is not that much different from the tropical grid size of the analysis fields, there would appear to be little subgrid scale features to be removed from the grid-point values.

IV. ANALOG TRACK FORECASTS BY MAP TYPES

With each map now typed, a forecast position is derived. The following procedure is simple and later can be greatly refined, as indicated in the next chapter. As indicated in the introduction, the object here was not to optimize the technique, but rather to see if a representative forecast could be made based on the map types.

Before any comparison of forecast positions could be made, all the positions had to be standardized. The 0-hour position, or map time position, of the storm is converted to 10° N and 140° E. This position is arbitrary and does not affect the results. It only serves as a reference position. All other best-track positions are then converted to a latitude/longitude position relative to this reference position. Then, each case is selected in succession. All other cases in its same map type serve as forecast analogs. Before the forecast positions are actually derived, all the best-track positions are rotated about the 0-hour storm position so that each analog has the same direction of movement for the 12 hours prior to map time. There are no restrictions placed on this rotation. The equations that accomplish this rotation are,

$$CALAT = SLAT + (PALAT-PSLAT) \cdot FCST/12$$
$$CALON = SLON + (PALON-PSLON) \cdot FCST/12$$

where CALAT and CALON represent the rotated analog latitude and longitude; SLAT and SLON represent the unrotated analog latitude and longitude; PALAT and PALON represent the prior 12-hour analog latitude and longitude; PSLAT and PSLON represent the prior 12-hour current case latitude and longitude; and FCST represents the forecast interval, i.e. 30, 36, 54, 60, 78 and 84 hours. It also assumes that changes in latitude and longitude by an equal increment represent a true distance.

All rotated analog storm positions within the same map type (excluding the map for the case being forecast) are then averaged, and this average storm position becomes the forecast position for that case. These forecast positions are compared against the actual standardized best-track position. A mean error and standard deviation are computed for each map type and for the full 504 case sample. A summary of the results for the full sample is provided in Table III. See Appendix C for the map type summaries for 700 and 850 mb levels.

It was hoped that this study would show that the easy to forecast situations could be separated from the difficult ones, and a quantitative estimate of forecast accuracy could be made. In a limited sense this can be shown in Table IV by comparing map type 2 and 3. The mean error and standard deviation for map type 2 are less than those for map type 3

TABLE III

Summary of mean forecast errors (n.mi.) and standard deviations (n.mi.) for the analog-type forecast.

Fcst Int	850 mb Mean	850 mb Std Dev	700 mb Mean	700 mb Std Dev	500 mb Mean	500 mb Std Dev
30	137.9	93.3	137.9	93.2	138.2	95.0
36	175.6	119.7	175.2	119.6	175.8	121.8
54	289.3	180.1	292.3	188.1	284.4	183.5
60	332.3	207.3	333.1	218.1	326.2	211.4
78	456.4	287.2	460.4	282.1	452.0	288.9
84	492.0	317.5	484.2	321.1	497.8	338.1

in every forecast time interval. This would indicate that storms in map type 2 are easier to forecast (by this analog procedure) than those of map type 3. Based on the maps in Fig. 8, most forecasters would probably agree with this assessment. However, a test with independent data after optimizing the technique will give a much better indication of the significance of this concept. It does show that the potential exists.

It is obvious from the average errors, as presented in Tables III and IV, that the results do not represent any major breakthrough. However, it must be remembered that the techniques have not been optimized and many refinements (see Chapter V) can be applied that should give better forecasts. In any case, the errors are not that bad when compared to the official forecast errors and represent a solid base from which to build. The official forecast errors for the specific cases in this study are not known. A rough estimate

TABLE IV

Mean forecast errors (n.mi.) and standard deviations (n.mi.) by 500 mb map type and forecast interval.

MAP TYPE	30-HR MEAN	30-HR STANDARD DEVIATION	30-HR NUMBER OF CASES	36-HOUR MEAN	36-HOUR STANDARD DEVIATION	36-HOUR NUMBER OF CASES	54-HR MEAN	54-HR STANDARD DEVIATION	54-HR NUMBER OF CASES
1	130.1	93.6	156	163.3	114.9	145	266.3	172.9	132
2	116.0	85.6	84	148.3	108.0	82	238.4	177.1	68
3	148.8	97.6	58	181.9	113.7	55	327.0	193.1	46
4	123.6	70.6	45	165.2	98.0	43	275.8	136.7	35
5	144.2	82.1	43	184.0	108.5	42	294.4	136.7	38
6	137.8	80.7	31	190.3	113.4	27	370.2	235.4	17
7	147.8	103.4	20	190.0	134.8	19	251.2	162.9	14
8	154.0	82.5	16	211.3	106.4	14	419.3	233.0	10
9	198.8	146.5	28	270.1	201.3	25	387.0	193.1	11
10	158.4	90.7	13	195.1	139.2	10	241.7	115.8	7
11	156.8	93.6	10	195.5	109.5	10	316.2	186.3	9
TOTAL	138.2	95.0	504	175.8	121.8	482	284.4	183.9	387

MAP TYPE	60-HR MEAN	60-HR STANDARD DEVIATION	60-HR NUMBER OF CASES	78-HR MEAN	78-HR STANDARD DEVIATION	78-HR NUMBER OF CASES	84-HR MEAN	84-HR STANDARD DEVIATION	84-HR NUMBER OF CASES
1	307.5	196.8	127	442.9	227.1	107	482.6	296.3	100
2	276.2	215.8	62	392.8	277.9	47	423.8	294.1	42
3	382.5	235.2	43	553.7	349.1	28	596.8	423.8	26
4	329.9	157.3	32	451.3	261.3	26	469.5	295.7	23
5	337.0	227.2	34	337.7	231.5	25	507.0	475.1	24
6	398.9	221.6	16	565.0	278.9	12	665.5	295.1	10
7	284.2	185.1	13	429.0	205.5	10	432.6	190.1	9
8	448.4	232.7	9	682.6	330.8	4	769.0	371.1	4
9	444.3	196.8	8	662.1	292.6	3	729.7	352.4	3
10	280.7	138.5	7	408.3	285.5	5	452.6	312.9	5
11	352.5	232.2	9	615.9	357.1	6	461.2	187.6	4
TOTAL	326.2	211.4	360	452.0	288.9	273	497.8	338.1	250

of the official JTWC warning error was computed by taking the mean error for each of the years included in this study, summing them and dividing by the number of years (10). The results indicated an average error of 112 n.mi. at 24 hours, 229 n.mi. at hours, and 347 n.mi. at 72 hours. These average errors include all warnings issued for storms of tropical storm intensity for the time frame involved.

Another question regards the level that gives the best steering motion. It is obvious from Table III that the data from all three levels produced remarkably similar errors. Why this occurred is uncertain, but it is conjectured that the adjustment made for the past 12-hour motion strongly influenced these average error statistics. To further examine how the schemes at each level performed, a block of 20 storms was selected at random from the data sets and presented in Table V. The data at each level for these storms is remarkably consistent, which may again be the result of the corrections made for the past 12-hour movement.

TABLE V.

Examples of 30-hour forecasts made at 850, 700 and 500 mb. All positions are relative to the standardized 0-hour position (10° N, 140° E) and given as lat/long (map type number).

CASE NUMBER	850 MB	700 MB	500 MB	ACTUAL
375	14.8/143.8 (8)	13.7/142.6 (4)	13.7/142.6 (3)	11.9/144.2
376	14.0/133.2 (5)	13.7/134.2 (2)	13.7/133.7 (3)	10.5/133.5
377	13.1/142.4 (3)	13.6/141.6 (3)	13.1/141.5 (2)	12.8/136.3
378	9.1/143.3 (3)	9.1/142.4 (1)	9.2/142.7 (1)	9.8/136.3
379	12.9/139.7 (5)	12.7/140.8 (2)	12.6/140.3 (4)	13.0/144.3
380	14.7/143.1 (4)	14.2/142.2 (4)	14.8/142.0 (9)	13.5/144.3
381	13.8/135.9 (12)	13.9/136.8 (4)	12.9/136.4 (10)	15.6/140.7
382	15.1/138.6 (12)	15.6/138.6 (3)	15.2/138.7 (1)	12.9/136.5
383	13.8/137.9 (3)	13.7/137.6 (4)	13.6/137.6 (3)	15.0/138.4
384	12.5/139.1 (1)	12.4/139.2 (1)	12.3/139.3 (2)	12.0/139.5
385	10.7/138.9 (1)	10.6/139.0 (1)	10.6/139.0 (2)	11.9/140.0
386	14.7/140.2 (1)	14.6/140.3 (1)	14.6/140.3 (2)	15.7/134.0
387	15.4/131.5 (5)	13.6/131.4 (11)	15.8/132.6 (7)	16.1/133.8
388	10.2/136.1 (1)	10.6/136.3 (3)	10.1/136.3 (2)	12.3/137.2
389	13.0/138.0 (2)	13.1/137.8 (1)	13.2/138.0 (1)	13.5/136.2
390	12.8/135.6 (2)	12.9/135.3 (1)	13.4/136.5 (7)	11.0/137.8
391	10.3/139.5 (2)	10.4/138.8 (5)	10.5/139.5 (1)	10.2/140.3
392	11.8/142.1 (6)	11.7/142.0 (5)	11.7/142.6 (1)	11.5/138.5
393	11.5/141.2 (2)	11.7/140.5 (5)	11.7/141.2 (1)	10.5/139.1
394	11.3/139.8 (2)	11.2/140.6 (2)	11.3/139.6 (2)	11.7/139.3

V. SUGGESTED IMPROVEMENTS

Since this was an initial study to verify that the techniques would work, several procedures were not optimized. The first procedure that needs this optimization is the EOF truncation procedure, using the Preisendorfer and Barnett (1977) method. In Chapter III we noted that the 20 term EOF map types show considerably more detail than the ones attempted with 10 terms. Whether this additional detail is desirable or not (i.e., whether it is "signal" or "noise") remains to be proved. We suspect that the motion of the tropical storm is primarily dependent on the large-scale synoptic situation, and the 10 term EOF map types may have represented these large-scale features well enough to distinguish the map types. Unfortunately, it is also possible that some of the first 10 terms of the EOF may actually be "noise". Thus, there may be too many terms in the EOF. Table VI contains the 30-hour forecast results using the 20 terms. The average error for the entire sample does not show any improvement, but it does show a wider range of average errors for the specific map types. Therefore, by using more terms it may be possible to better separate the easy forecasts from the difficult ones. Remember that this suggestion was made on the basis of the forecasts for one

level and one forecast interval. More data must be gathered before this idea can be really supported or refuted.

TABLE VI

30-hour forecast mean errors (n.mi.) and standard deviations (n.mi.) at 500 mb using 20 terms of the EOF.

Map Type	Mean	Standard Deviation	Number of Cases
1	141.2	100.3	173
2	125.5	75.4	49
3	130.1	106.2	65
4	110.6	68.9	30
5	119.0	65.9	37
6	170.0	103.7	24
7	133.4	79.9	19
8	130.2	83.4	22
9	147.2	108.8	17
10	184.3	109.4	15
11	147.7	90.0	11
12	236.7	39.8	4
13	75.3	42.2	11
14	216.2	123.3	6
15	157.1	71.7	7
16	145.6	48.4	6
17	222.4	117.6	6
18	-----	-----	2
Total	139.6	97.1	504

Also, as indicated at the beginning of Chapter III, once the proper truncation point has been determined an attempt should be made to use the eigenvectors as the map types. This use of the eigenvectors should work as well or better than the characteristic map type approach and has the advantage of much fewer computations. However, this procedure would work only for the map-typing scheme and would not work for the strictly analog scheme suggested later in this chapter.

Next, if the map-typing concept is to be followed, a weighted average should be used to compute the forecast positions. The weighting function should be inversely proportional to the least squares distance from each map in the map type to the case being forecast. This procedure would give more weight to the positions from the maps that most closely resemble the present case. In other words, the more similar the maps are, the more likely the synoptic forcing is similar. Therefore there is a higher probability that the future movements will be similar. Thus the forecast should be improved.

The past 12-hour movements should also be compared before using all the cases in the map type to compute a forecast movement. Any case within the map type that does not have a similar past movement, within say plus or minus 30-40 degrees, should not be included when computing the forecast position. The justification for this procedure is that if the past 12-hour movement is so much different than the current case, the forcing mechanisms for the two cases are most likely different. This could be due to rapidly changing patterns or to small-scale features in the synoptic situation that the map-typing scheme did not resolve. Later versions of the analog forecast scheme of Jarrell and Somervell (1970) use a similar restriction on permissible past-motion vectors in the analog scheme.

Another improvement to the methodology that should improve the selection of the map types is to devise a more statistically significant means of selecting the least squares distance than the trial and error method used here.

Another more radical change to the procedure would offer the potential for still greater improvements. This would be to vary the size of the domain based on the forecast interval. Thus the domain would be smaller for the 30-hour forecast than the 84-hour forecast. In this study only one grid domain was used for all forecast intervals. By varying the domain size we can select the features that affect the movement in the interval. For example, with the domain used in this study, the variance expressed by features at the extreme edge of the domain (2400 n.mi. away) may have no influence on the 30-hour movement, but may be very significant in the longer time frames. The proposal here would be to shrink the domain for the 30-hour and 36-hour forecasts, in order for the EOF procedure to maximize the variance in the area that is most likely to affect the storm's movement in that time interval.

Another possibility is to revert to a strictly analog technique, in which each of the 504 cases is treated as a potential analog. Instead of having predetermined map types, simply select the 10 best fits, in the least squares sense, to the present map. Then use these 10 best fits to

compute the forecast position. This would perhaps give a better forecast position, but it would not have the advantage of having a predetermined estimate of the accuracy of the forecast based on the map types.

VI. SUMMARY

The objective of this initial study was to use the hypothesis that tropical storm motion is directly related to the forcing of the synoptic height fields, and to construct map types around the tropical storm that represent this forcing. After this forcing, represented by the map types, is determined, we then use it to derive forecast storm positions.

First, the FNOC analysis fields are interpolated to a standard grid based on the tropical storm position. Then the maps are organized into a matrix and an EOF analysis is completed. The EOF are then truncated in an effort to eliminate noise and the subgrid scale phenomena. The time coefficients of the truncated EOF are used to compare the maps in eigenvector space. A least squares procedure is used for these comparisons. The maps are highly correlated and will tend to form in clusters in the eigenvector space. By identifying these clusters and picking the maps that are most representative of each of these clusters, the map typing is accomplished. The map types are then used to divide the 504 individual cases into groups. The maps in each group represent similar synoptic situations, which can be used to derive forecast storm positions. The forecasts

are developed by using the known best-track positions of the storms in each map type and rotating them so that they have the same past 12-hour movement as the case currently being forecast for. An average position from the map type is then used as the forecast.

This research shows that the concept is valid. The procedures involved need to be optimized and refined. Map types can indeed be formed using the EOF analysis and least squares statistics. The forecast movement errors arrived at in this study, do not appear to be as good as the official forecast, but since the technique was not optimized, they were not expected to be as good. The fact that the errors in this research were as close to the official forecast errors as they were, indicates that further refinement of the technique is warranted. By optimizing the procedures and employing some of the refinements from Chapter V, this technique should be able to equal or better the official forecast.

APPENDIX A

Methods for representing arrays of environmental fields by empirical orthogonal functions have been formulated in a number of different ways (for example Lorenz (1956), Freiberger and Grenander (1965), Kutzbach (1967), Essenwanger (1976), and Little (1980)). Most of the information presented in this appendix is based on the work of Kutzbach (1967) as presented by Little (1980).

Let A be an M component vector that represents the nth (n=1,...,N) observation. Let A be an M by N matrix, where the nth column is the observation vector A_n. The goal is to determine a vector e which has the highest degree of similarity to all the A_n vectors. Kutzbach (1967) explains that the similarity is measured with the squared normalized inner product of the observation vectors A_n and the vector e. After averaging over all of A, the problem is to maximize

$$(e'A^2)N^{-1}/e'e = \frac{(e'A)(e'A)'}{Ne'e} = \frac{e'AA'e}{Ne'e} \qquad (1\text{-}1)$$

where the prime denotes the transpose. This is equivalent to maximizing,

$$e'Be$$

where B represents the normalized symmetric (M x M) covariance matrix, and is subject to the conditions

$$e'e = 1 \tag{1-2}$$

and

$$B = N^{-1}[A'A] \tag{1-3}$$

Furthermore, Kutzbach (1967) points out that the maximization of (1-1) subject to (1-2) leads to the equation

$$Be = e\lambda \tag{1-4}$$

The vector e and the parameter λ are recognized as an eigenvector and associated eigenvalue of B. It can be shown that the e are orthogonal and that the λ_i are real and positive. Thus for the whole matrix, (1-4) can be written as

$$BE = EL \tag{1-5}$$

where E is the M x M eigenvector matrix and L is the M x M diagonal eigenvalue matrix. Also note that

$$E'E = 1 \tag{1-6}$$

It is now assumed that the elements of L and the respective columns of E have been arranged such that λ_1 is the largest λ and λ_2 is the next largest λ, etc. From (1-6) the transpose of an orthogonal matrix is equal to its inverse. Thus combining (1-3) and (1-5), the result is

$$E'AA' = LN$$

Now define C = E'A, where C is an M x N matrix. It follows that

$$A = EC$$

and

$$A_n = \sum_{i=1}^{M} C_{in} e_i \ , \ n=1,\ldots,N \qquad (1\text{-}7)$$

Thus from (1-7), the observation vector A_n can be expressed as a linear combination of the m eigenvectors and n C vectors or coeffficient vectors. If the entire E and C matrices are used the exact data matrix A can be reproduced.

In most applications to meteorological fields, where the data vectors A are highly correlated, it is found that a large portion of the variance (λ) can be accounted for by retaining only the first few of the largest eigenvalues (λ) and eigenvectors (e). Thus by retaining only the first few terms of (1-7), an excellent representation of the observation can be obtained, with the rest of the terms being considered noise. Thus if an A_n^* is defined as the approximation of the nth observation vector then

$$A_n^* = \sum_{i=1}^{M^*} C_{in} e_i \ , \ n=1,\ldots,N \ M^* < M$$

This allows for truncation of the noise by removing the terms with small variance (λ) as shown by Preisendorfer and Barnett (1977).

APPENDIX B

The following is the sequence of operations/computer routines that were used on the data array to accomplish the Empirical Orthogonal Function analysis and to produce the "noise-free" data:

ARRAY	NAME	COMPUTER ROUTINE
A (120,504)	Anomalous Data Set	
B (120,120) = AA'	Normalized Symmetric Covariance Matrix	VTPROF
L (120,120)	Eigenvalues	EIGRS
E (120,120)	Eigenvectors	EIGRS
C (120,504) = E'A	Time Coefficients	VMULFM
E^*(120,10)	Truncated Eigenvectors	
C^*(10,504)	Truncated Time Coefficients	
A^*(120,504) = E^*C^*	Approximated Data Set	VMULFM

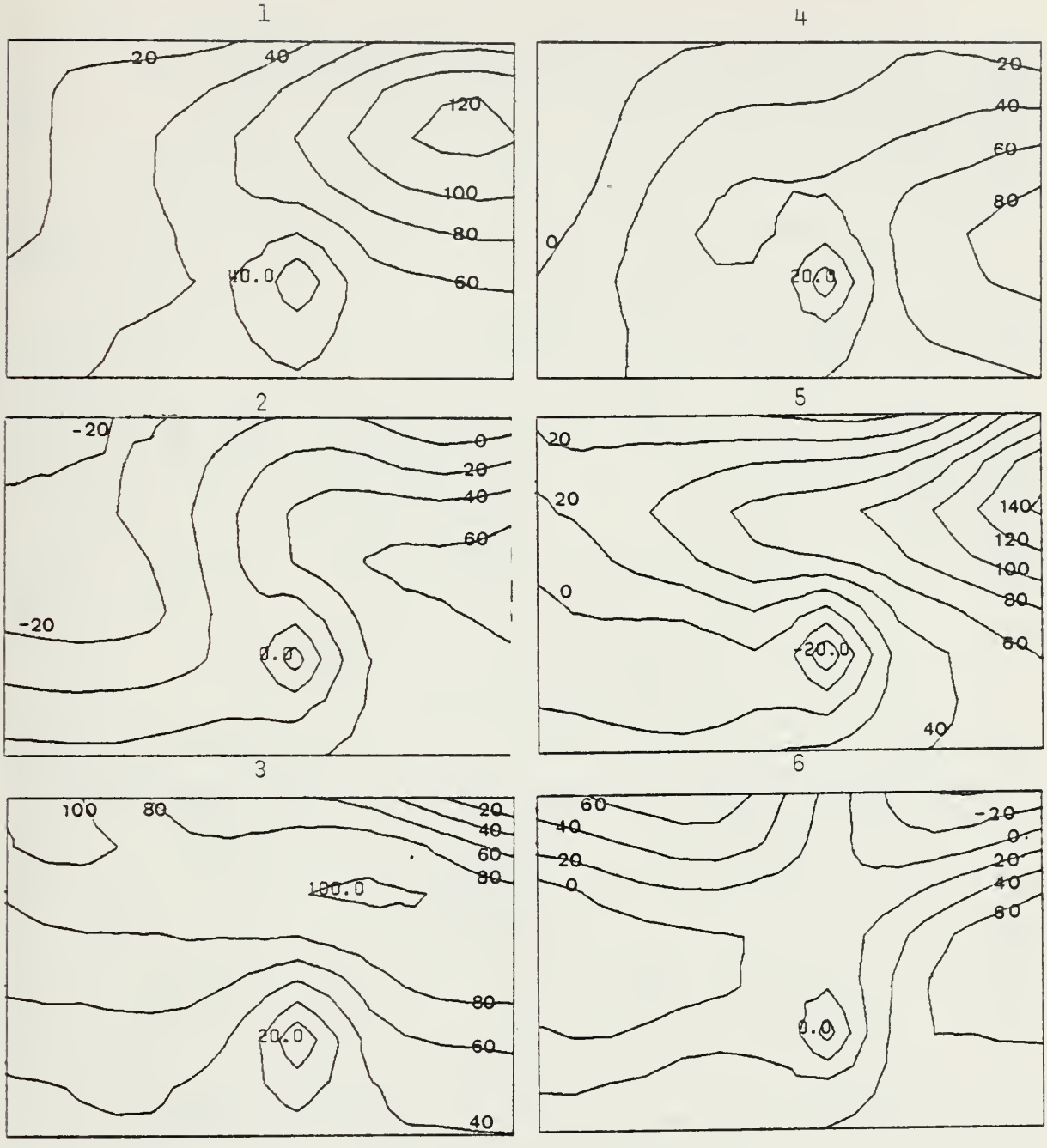

Figure C1. 850 mb map types 1-6. Isopleths are D-values (m).

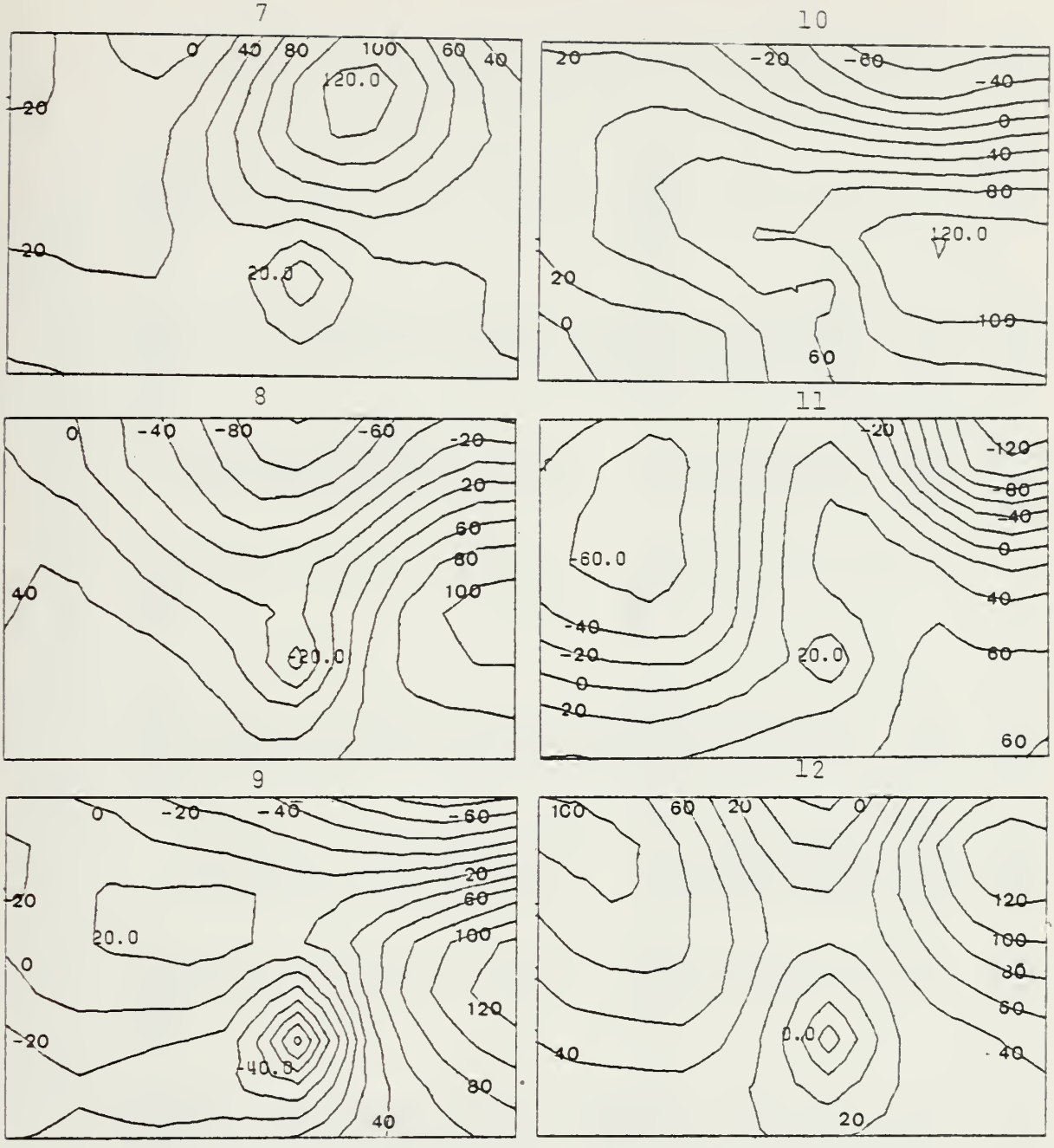

Fig. C1. cont. 850 mb map types 7-12.

TABLE C1. 850 mb errors and standard devisions (n.mi.) by map type and forecast interval.

MAP TYPE	30-HR MEAN	30-HR STANDARD DEVIATION	30-HR NUMBER OF CASES	60-HR MEAN	60-HR STANDARD DEVIATION	60-HR NUMBER OF CASES	54-HR MEAN	54-HR STANDARD DEVIATION	54-HR NUMBER OF CASES
1	133.2	99.6	111	167.3	126.8	110	266.9	164.3	100
2	123.3	87.7	101	156.4	106.1	99	261.0	161.0	79
3	150.0	103.8	91	189.0	127.7	89	295.6	187.5	71
4	128.9	80.8	56	161.5	102.2	51	289.2	202.8	38
5	138.6	92.9	42	173.5	116.3	41	296.5	200.6	34
6	162.8	110.0	22	210.2	166.7	18	356.6	141.7	11
7	137.8	66.8	21	178.9	83.8	21	309.3	140.1	21
8	142.1	68.7	15	203.1	92.4	13	277.6	97.8	5
9	125.6	74.0	14	148.3	81.7	12	281.0	97.0	9
10	145.9	79.7	11	198.9	102.9	10	364.8	190.2	6
11	169.1	69.0	7	255.0	130.0	5	584.7	268.0	3
12	186.6	89.5	13	258.4	129.0	13	431.7	226.3	10
TOTAL	137.9	93.3	504	175.6	119.7	482	289.3	180.1	387

MAP TYPE	60-HR MEAN	60-HR STANDARD DEVIATION	60-HR NUMBER OF CASES	78-HR MEAN	78-HR STANDARD DEVIATION	78-HR NUMBER OF CASES	80-HR MEAN	80-HR STANDARD DEVIATION	80-HR NUMBER OF CASES
1	302.5	185.8	98	413.8	258.8	79	442.9	284.5	73
2	298.7	182.8	75	429.1	272.0	56	445.8	281.1	51
3	354.9	239.0	62	442.0	248.7	47	478.5	281.8	43
4	321.7	228.0	33	512.8	320.8	21	570.3	410.6	17
5	335.4	218.6	33	469.2	270.4	28	539.1	300.0	27
6	400.6	173.4	11	537.8	327.9	8	502.8	213.0	7
7	349.7	147.7	19	469.2	240.0	16	452.1	205.4	15
8	410.3	141.0	4	-	-	0	-	-	-
9	354.4	91.9	9	532.9	296.0	5	614.9	330.0	5
10	458.5	227.0	5	584.7	332.3	5	818.8	236.1	4
11	-	-	2	-	-	1	-	-	1
12	552.0	292.3	9	764.4	537.7	7	852.5	637.7	7
TOTAL	332.2	207.3	360	456.4	287.2	273.	492.0	317.5	250

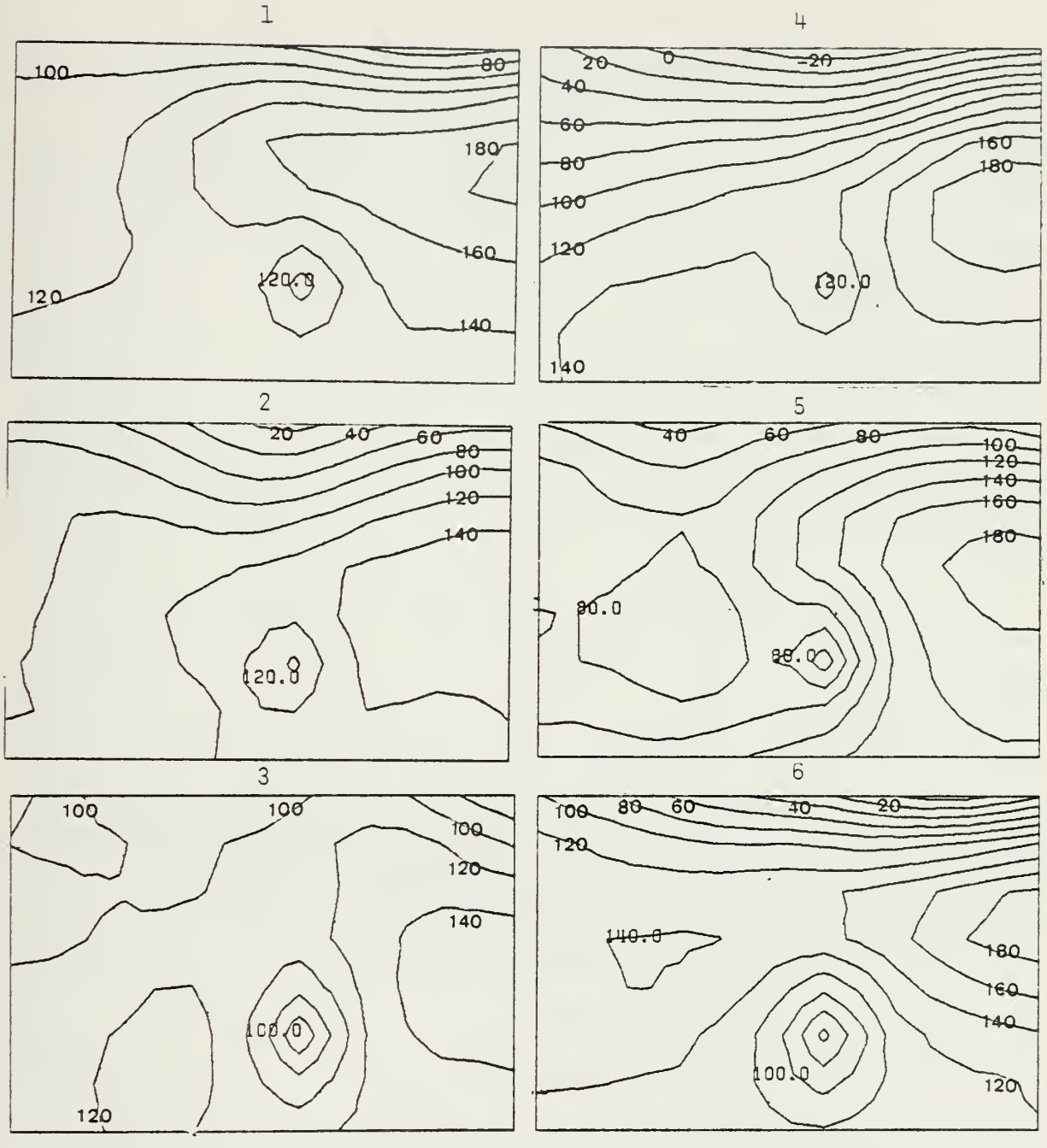

Figure C2. 700 mb map types 1-6. Isopleths are D-values (m).

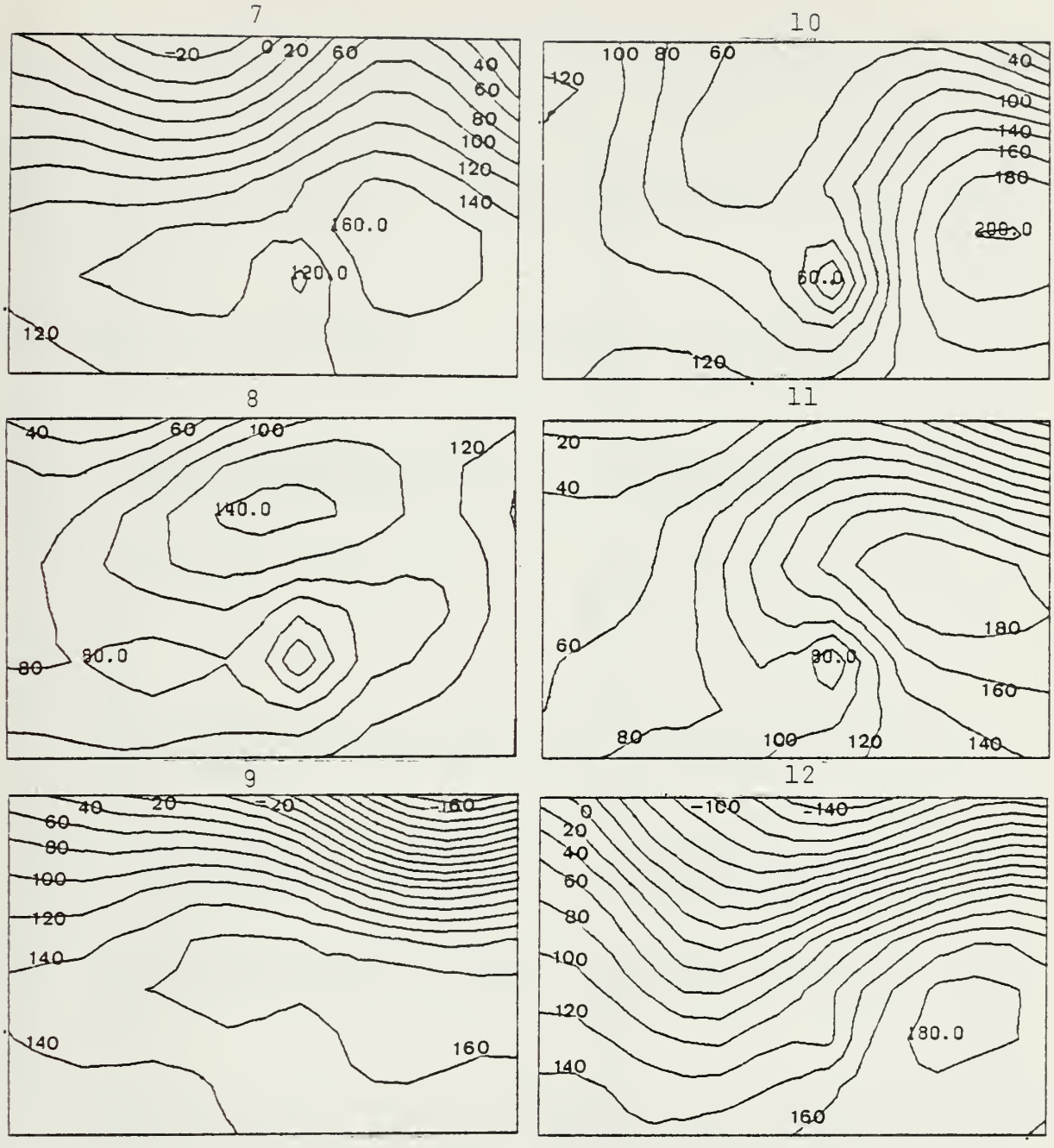

Fig. C2. cont. 700 mb map types 7-12.

TABLE C2. 700 mb errors and standard deviations (n.mi.) by map type and forecast interval.

MAP TYPE	30-HR MEAN	30-HR STANDARD DEVIATION	30-HR NUMBER OF CASES	36-HR MEAN	36-HR STANDARD DEVIATION	36-HR NUMBER OF CASES	54-HR MEAN	54-HR STANDARD DEVIATION	54-HR NUMBER OF CASES
1	132.8	94.1	133	163.8	113.3	130	278.6	185.3	119
2	122.2	78.7	113	154.6	105.3	108	259.1	149.4	84
3	140.5	85.5	66	174.9	110.4	65	280.8	170.1	49
4	130.7	120.0	40	175.5	141.7	38	281.5	166.4	30
5	156.4	98.6	44	201.2	129.5	43	329.9	182.9	33
6	111.6	52.5	28	151.9	62.9	25	244.9	104.1	22
7	104.3	148.3	20	177.8	101.0	17	323.4	175.6	13
8	165.4	122.4	22	211.5	161.7	22	272.5	157.0	17
9	189.8	100.3	13	252.6	124.4	11	466.8	304.4	8
10	144.0	71.4	9	187.3	109.4	8	-	-	2
11	217.6	114.7	12	267.3	144.4	12	492.0	228.2	9
12	139.8	73.2	4	266.1	140.5	3	-	-	1
TOTAL	139.8	93.2	504	175.2	119.6	482	287.4	179.8	387

MAP TYPE	60-HR MEAN	60-HR STANDARD DEVIATION	60-HR NUMBER OF CASES	78-HR MEAN	78-HR STANDARD DEVIATION	78-HR NUMBER OF CASES	84-HR MEAN	84-HR STANDARD DEVIATION	84-HR NUMBER OF CASES
1	316.4	211.7	106	439.8	275.1	101	456.6	288.6	96
2	302.4	178.6	78	471.3	234.2	59	530.3	339.9	48
3	310.5	193.8	46	398.2	249.5	36	396.1	253.2	31
4	316.6	203.1	28	478.6	395.4	19	512.6	453.5	18
5	342.9	196.9	31	417.1	236.5	21	439.2	284.4	21
6	339.1	175.5	19	449.2	167.9	13	482.6	205.0	13
7	363.0	210.2	11	621.8	354.4	6	646.2	380.5	6
8	329.1	182.0	15	510.0	240.1	11	465.7	193.8	10
9	658.2	378.9	6	1052.4	377.3	4	1112.6	378.6	4
10	-	-	2	-	-	-	-	-	-
11	463.4	219.3	7	628.7	283.9	3	595.4	270.9	3
12	-	-	1	-	-	-	-	-	-
TOTAL	317.8	203.1	360	460.4	282.	273	484.2	321.1	250

APPENDIX D

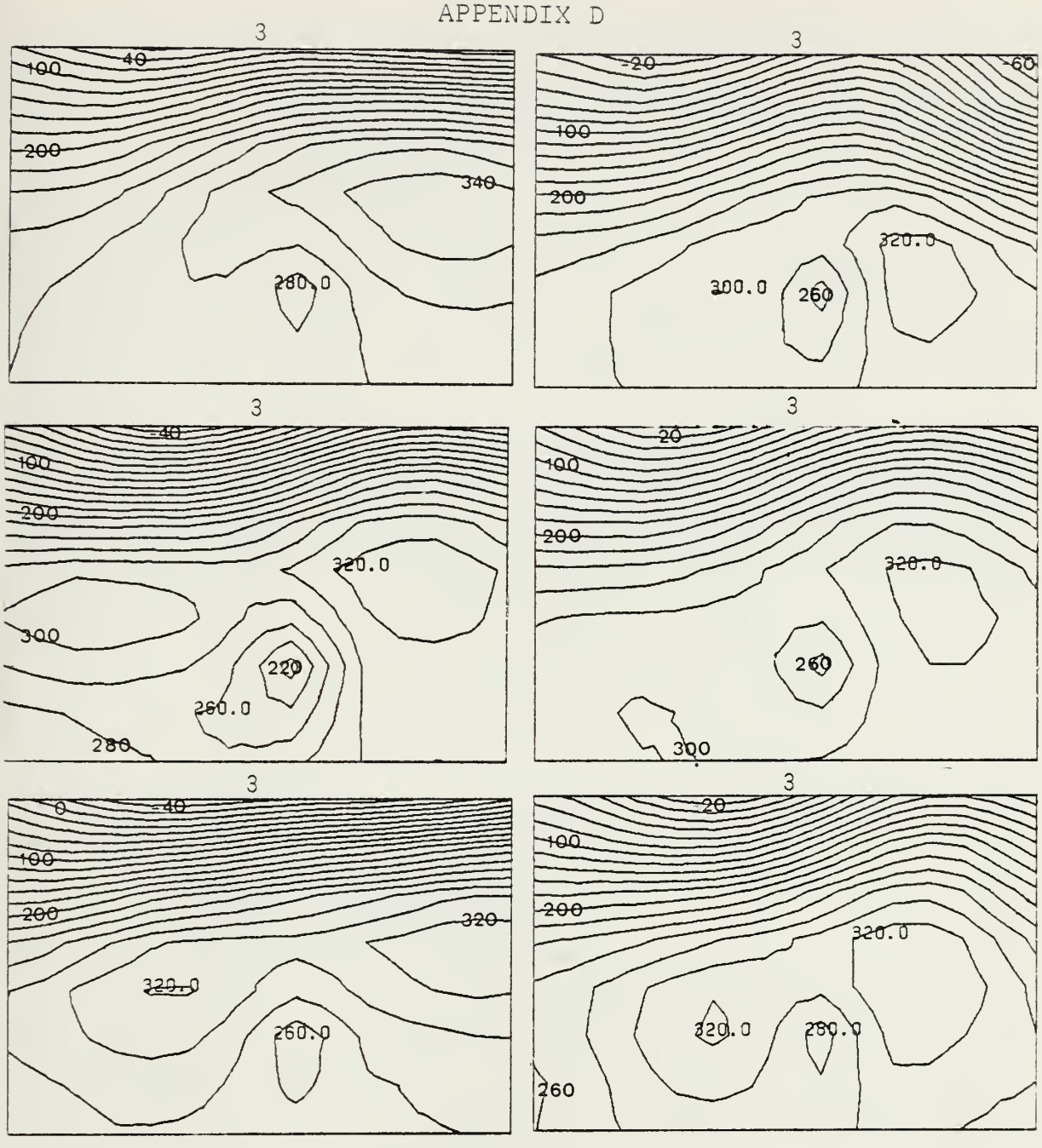

Figure D1. Examples of 500 mb maps. Isopleths are D-values (m) and the classification by map type is indicated by the number above the map.

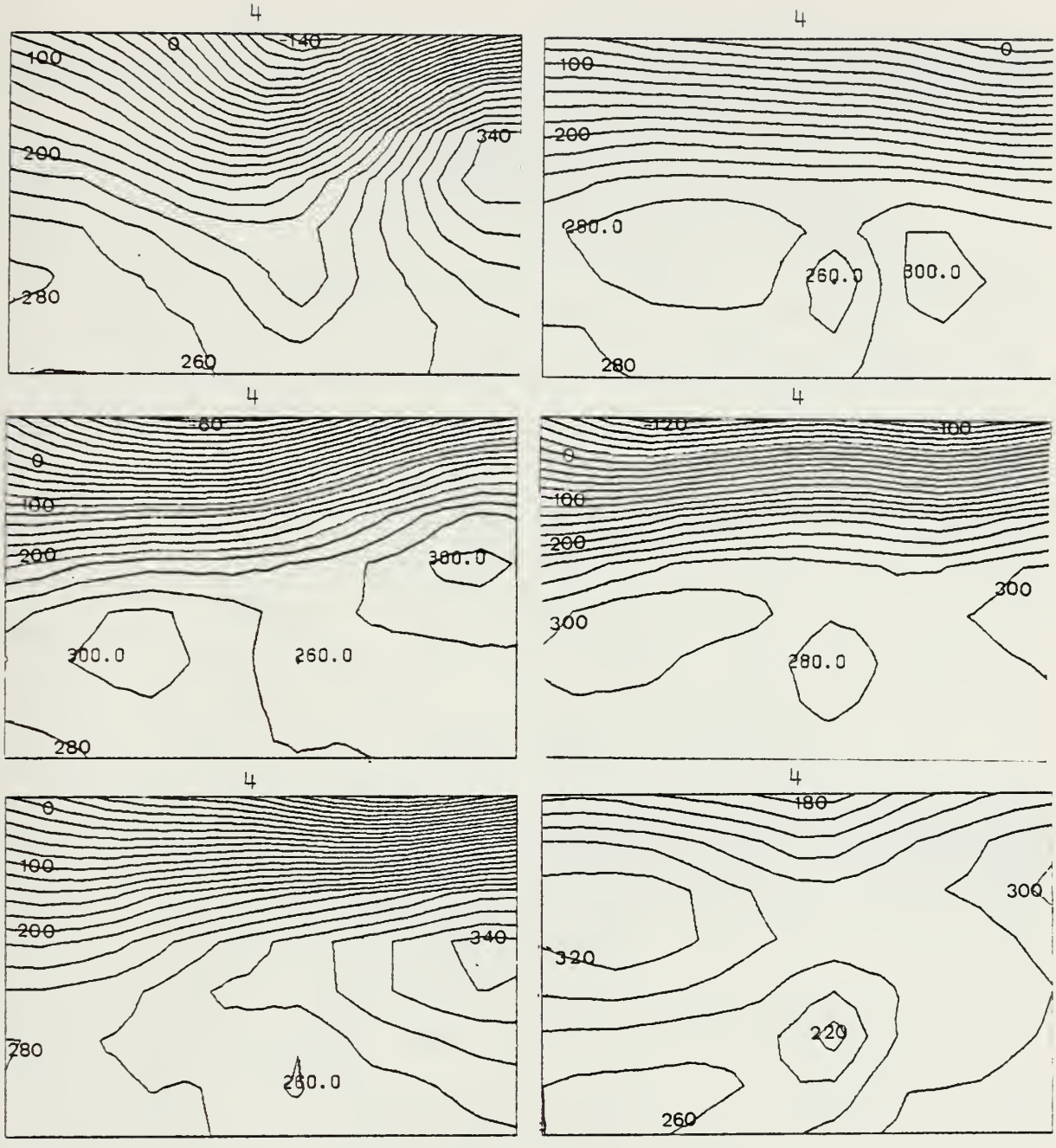

Fig. D1. cont. Examples of map type 4.

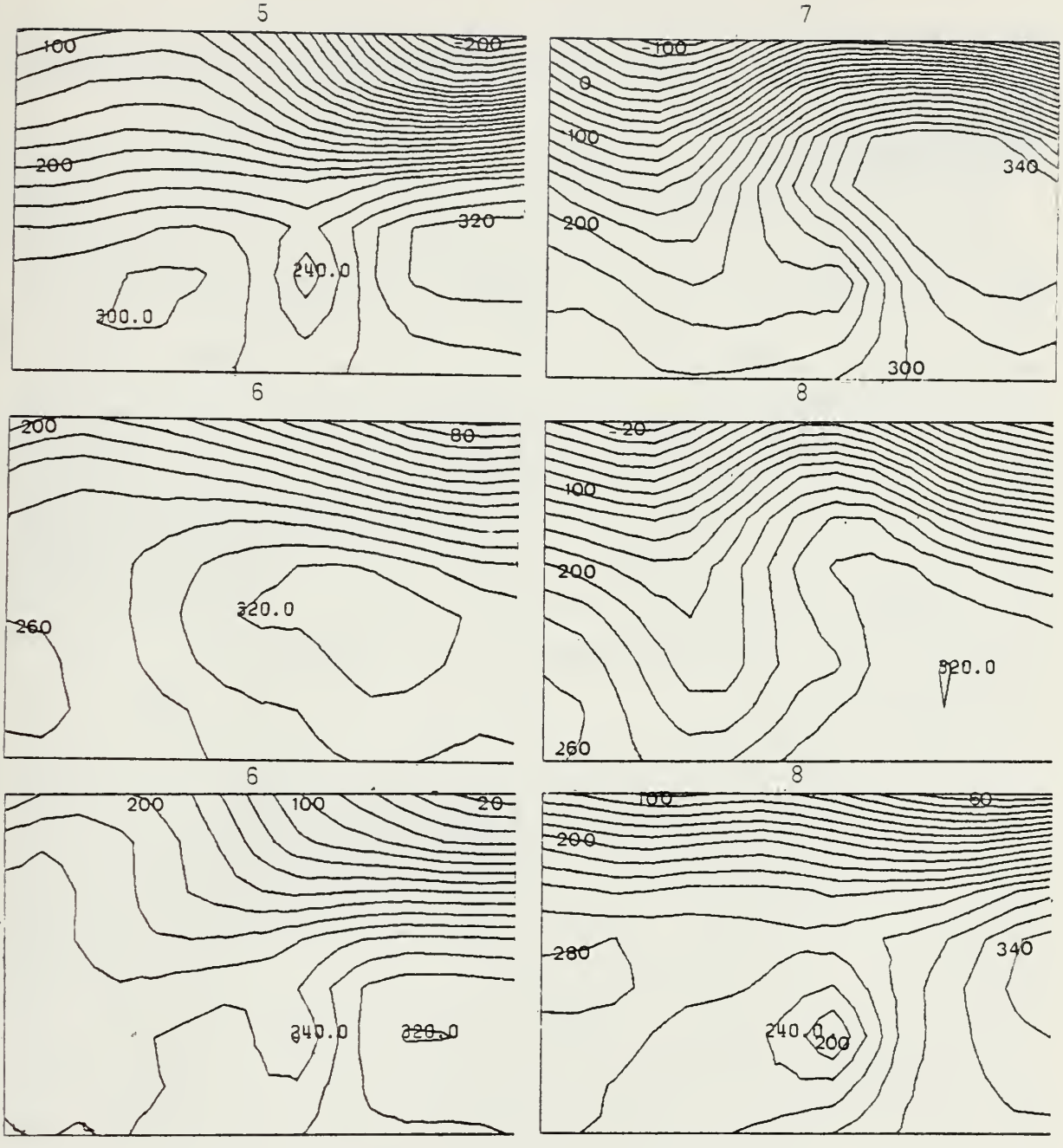

Fig. D1. cont. Examples of map types 5-8.

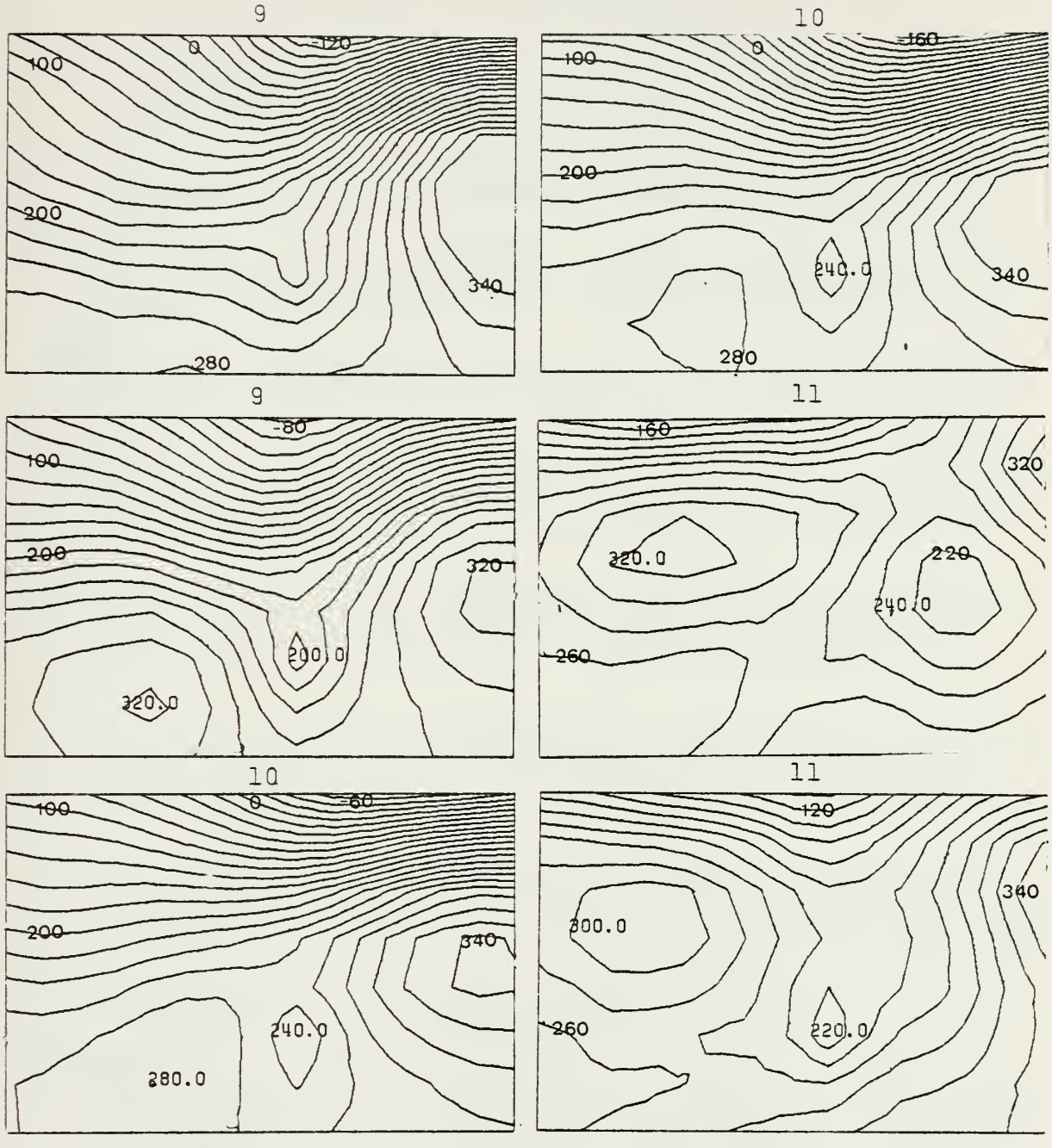

Fig. D1. cont. Examples of map types 9-11.

LIST OF REFERENCES

Annual Typhoon Report, 1976: U.S. Fleet Weather Central/ Joint Typhoon Warning Center, Guam.

Essenwanger, D., 1976: Applied Statistics in Atmospheric Science, Elsevier Scientific, Amsterdam, 412pp.

Freiberger, W. and U. Grenander, 1965: On the formulation of statistical meteorology. Review International Statistical Institute, 33, 59-86.

Hope, J. R., and C. J. Neumann, 1970: An operational technique for relating the movement of existing tropical cyclones to past tracks. Mon. Wea. Rev., 98, 925-933.

Jarrell, J. D., and W. L. Somervell, Jr., 1970: A computer technique for using typhoon analogs as a forecast aid. NAVWEARSCHFAC Technical Paper No. 6-70, 47pp.

Kutzbach, J. E., 1967: Empirical eigenvectors of sea-level pressure, surface temperature and precipitation complexes over North America. J. of Appl. Meteor., 6, 791-802.

Little, W. H., 1980: A statistical study of monthly storminess and sea surface temperature anomalies over the North Pacific Ocean. M.S. Thesis, Naval Postgraduate School, Monterey, California, 81pp.

Lorenz, E. N., 1956: Empirical orthogonal functions and statistical weather prediction. M.I.T., Department of Meteor., Sci. Rept. No. 1, Contract AF19(604)-1566, 49pp.

Lund, I. A., 1963: Map-pattern classification - by statistical methods. J. of Appl. Meteor., 2, 56-66.

Neumann, C. J., 1979: Statistical techniques. World Weather Watch WMO Tropical Cyclone Project - Sub-project No. 6, WMO-No. 528, Operational techniques for forecasting tropical cyclone intensity and movement, Chapter 4.

Preisendorfer, R. W., and T. Barnett, 1977: Significance tests for empirical orthogonal functions. 5th Conf. on Prob. and Statist. in Atmos. Sci., Nov 15-18, 1977, Amer. Meteor. Soc., Boston, MA, 169-172.

Tse, S. Y. W., 1966: A new method for the prediction of typhoon movement using the 700 mb chart. Quart. J. of the R. Met. Soc., April 1966, 239-253.

INITIAL DISTRIBUTION LIST

		No. Copies
1.	Defense Technical Information Center Cameron Station Alexandria, Virginia 22314	2
2.	Library, Code 0142 Naval Postgraduate School Monterey, California 93940	2
3.	Dr. Robert J. Renard, Code 63Rd Chairman, Department of Meteorology Naval Postgraduate School Monterey, California 93940	1
4.	Program Manager/CIRF Air Force Institute of Technology Wright-Patterson AFB, Ohio 45433	1
5.	Commanding Officer Fleet Numerical Oceanography Center Monterey, California 93940	1
6.	Commanding Officer Naval Environmental Prediction Research Facility Monterey, California 93940	1
7.	Commander Air Weather Service Scott AFB, Illinois 62225	1
8.	Commanding Officer Air Force Global Weather Central Offutt AFB, Nebraska 68113	1
9.	Dr. R. L. Elsberry, Code 63Es Department of Meteorology Naval Postgraduate School Monterey, California 93940	5
10.	Systems and Applied Sciences Corporation 570 Casanova Avenue Monterey, California 93940	1

11. Major Danley W. Brown 4
Air Force Global Weather Central/WF
Offutt AFB, Nebraska 68113

Thesis 193631
B80994 Brown
c.1 Tropical storm
movement based on
synoptic map typing
using empirical
orthogonal functions.
16 SEP 67 3 3 5 3 6
c

Thesis 193631
B80994 Brown
c.1 Tropical storm
movement based on
synoptic map typing
using empirical
orthogonal functions.

thesB80994
Tropical storm movement based on synopti
3 2768 002 07994 9
DUDLEY KNOX LIBRARY